Politecnico di Torino

Politecnico di Torino

Corso di Laurea Magistrale in Nanotechnologies for ICT's

Tesi di Laurea Magistrale

Synthesis and characterization of highly sensitive Polydimethysiloxane (PDMS) porous pressure sensors for wearable applications

A.a. 2023/2024

Dicembre 2023

Tutor:
Prof. Stassi Stefano

Candidate:
Costantini Matteo

Abstract

The recent development of Information Technologies requires to collect a large amount of multi-disciplinary data derived from humans' habits, social life and physical activities. Consequently, the need of new ways to interface rigid electronic devices with soft and flexible human tissues has drastically grown. Nowadays, wearable sensors and devices constitute the link between the two realms. Their application range is widespread, from medicine to military defense, and moreover they can sense a large variety of human signals, from hearth rate to anxiety. Among them, pressure is a transverse physical quantity to be sensed. Herein, a flexible sandwich-like pressure sensor composed of a Polydimethylsiloxane (PDMS) porous sponge, is presented. Two different synthesis methods were explored, whether using a common lump of sugar as sacrificial casting template or not. Moreover, both polymer-only samples and samples decorated with the addition of metal nanoparticles were investigated to study the impact on the device's performances. Each sensor was subjected to dynamic and static compression tests and its electrical properties variation was monitored by means of an LCR meter. The spongy sensors are characterized by negligible mechanical hysteresis over cycles of compression, relative capacitance variation up to 600 % and limit of detection down to half gram. Among all the type of sensors, the best one was used to build a small mat to map pressure in two dimensions. The results demonstrated that the sensors could be suitable for the development of customizable, lightweight, low-cost, and easy manufacturable wearable devices.

Contents

1 Introduction

The current Fourth Industrial Revolution is driven by the recent advances in artificial intelligence (AI) and internet of things (IoT), in which a lot of multidisciplinary data are continuosly collected and analyzed to infer new values from everyday life aspects [24]. During its physiological behaviors the human body produces a huge amount of varied data such as heart rate, temperature, blood pressure, voice, spatial position and limbs motion, stress level and mood, time spent in REM phase while sleeping etc. Many other complex informations which could be inputs for AI or IoT systems arise if one takes into account a person's social life, job, entertainment, eating habits, travels, purchases, mobility and so on. Consequently, a special class of electronic devices have to be intimately interfaced with people and their surroundings and be capable of sensing various stimuli. In this framework, wearable devices play an important role in terms of the measurement and collection of data [19]. Wearable sensors have evolved from body-worn fitness tracking devices to multifunctional, highly integrated, compact, and versatile sensors, which can be mounted onto the desired locations of our clothes or body to continuously monitor our body signals, and to better interact and communicate with our surrounding environment or equipment [12]. The global market for Internet of things (IoT) technology reached USD 100 billion for the first time in 2017, with a forecast to further grow to around USD 1.6 trillion by 2025 [24]. That's why in comparison to traditional bulky and rigid electronic devices, the human–machine interaction (HMI) system with flexible and wearable components is an inevitable future trend [26].
The range of applications of wearable and soft sensors is widespread since they are able to provide very in depth and useful insights about the wearer and the environment in several different scenarios. Possible opportunity areas are medicine, robotics, industry 4.0, videogames, military defense to name but a few. It has to be pointed out that the market is boosted by the growing interest in supporting healthcare, transitioning from a current hospital-centered one to a patient-centered ("medicine at home") one [17].
Point-of-care medicine currently uses implantable devices to endlessly register some patient vital signal, as done by the Continuos Glucose Monitor (CGM) showed in figure 1.

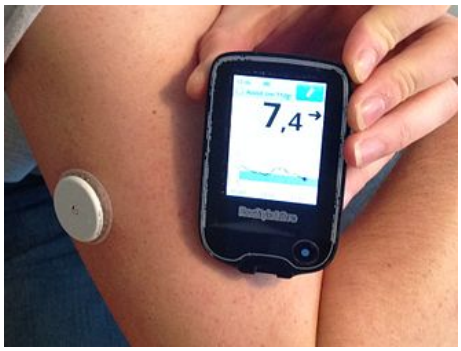

Figure 1 Continuos Glucose Monitor (CGM)

first approved in 1999. Applied on people with diabetes, the core of the CGM is an under skin electrode with an enzymatic technology which reacts with glucose molecules in the interstitial fluid generating an electrical signal then transmitted to a separate external receiver. CGM allows trends in blood glucose to be displayed over time instead of a single point to point like in traditional fingerprick test. New fascinating future healthcare implementations comes from research world too.

Davies et al. were inspired by the way the human skeletal muscles tune their morphologies to interact with the environment and have realized a novel hydraulic soft filament sensor (SFS), that transduces strain or force into hydraulic pressure changes thanks to the soft and stretchable micro-sized core filament filled with incompressible fluid [4]. If customized in a skin-like structure by weaving a single SFS with commercial yarn to form a planar fabric sensor (wearable garment) it becomes very effective for motion and gait constant monitoring (fig2).

Figure 2 Skin-like structure composed by an hydraulic soft filament sensor weaved with commercial yarn to form a planar fabric sensor (wearable garment)

Another possible application branch of soft sensors is Soft Robotics, a subfield of robotics concerning the design, control and fabrication of robots composed by compliant materials, instead of rigid links.

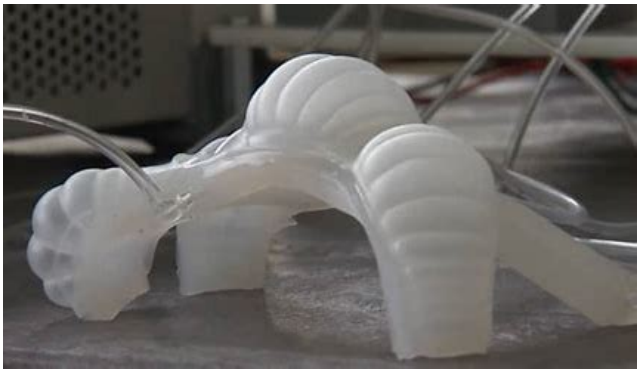

Figure 3 Example of soft robot

Robots with entirely soft bodies have tremendous potential, for example squeezing into places where rigid bodies cannot, which could prove essential in disaster relief scenarios. Sensors are one of the most important component of robots and, without surprise, soft robots ideally use soft sensors to detect stretch, bending, pressure and force.
Wearable suits fully provided with haptic feedback system are currently being commercialized for gaming, education, training in risky scenarios ecc. in VR environment. TeslaSuit (website https://teslasuit.io/) exploits electro muscle stimulation and transcutaneous electrical nerve stimulation to provide a full body haptic feedback and simulate a whole range of real-life feelings and sensations that may experienced on a immersive reality devices. Instead of a suit, Exit Suit (website https://exitsuit.com/) is an example of full-body rigid exoskeleton with a force-feedback potential, to totally submerge the user in the virtual experience.

An incredible portion of industrial wearable innovations is centered around safety and worker protection. Some workplace wearable safety devices able to prevent struck-by accidents and to reduce back injuries are set to change the modern production line. The GuardHat (website www.guardhat.com) is a Smart PPE (Personal Protective Equipment), that is an IoT helmet that tracks the location, pulse, body temperature of employees while monitoring their environment. The other major benefit of using industrial wearables is increased process efficency. Glove scanners like the ProGlove (website https://proglove.com/products/, fig4) are hands-free, lightweight scanner attached to the back of one's hand, saving up to 4-6 seconds per scan and reducing human errors by 33% (website https://vksapp.com/blog/industrial-wearables-changing-manufacturing).

Figure 4 ProGlove scanner

2 Soft pressure sensors

Wearable devices have such a pervasive and widespread range of applications thanks to the ability to be suitable for a lot of different scenarios and to detect and monitor a full range of signals, from heart rate to anxiety. Among them, pressure is a crucial physical quantity to be sensed in real-time health monitoring [13] but also in altimeter, drone, weather station, electronic cigarettes and so on [1]. A variety of feasible transduction mechanisms of pressure and, in general, of mechanical stimuli have been explored so far.

Kohli et al. developed a wearable magnetic-reluctance-based wireless pressure sensing module to measure intraoral pressure for clinical orthodontic treatment [14]. A sensing diaphragm is embedded into a wearable orthodontic aligner and placed inside the mouth, while a transmitting/receiving electromagnets (EM) are placed outside. When people use cheek muscle, pressure in the oral cavity is changed, so deflecting the sensing diaphragm toward or backward the above-mentioned EM. Consequently the magnetic reluctance between them is varied and then a voltage is electromagnetically induced in the receiving part. By analyzing the voltage output, the change of the pressure is known. The device was successfully proven to sense the change of the intraoral pressure when the thickness of the facial skin of a patient is less than 14 nm.

A powerful, non-invasive analytical tool for pressure sensing is light too. Li et al. proposed a wearable device consisting of a hybrid plasmonic microfiber knot resonator embedded in a polydimethylsiloxane (PDMS) membrane [15]. The working principle is based on the resonating wavelength shift under stretching and pressure and the sensing of wrist pulse, respiration and even finger pulse were experimentally proven.

Recently, a new pressure sensing approach utilizing the concept of "liquid-state electronics" has been introduced in which conductive liquids are embedded into elastomer microchannels. Deformation of the elastomers contributes to changes in the cross-section areas and length of the microchannels, resulting in changes in resistance along them. Gao et al. realized a microfluidic tactile diaphram pressure sensor based on embedded Galistan (alloy of gallium, indium and tin) microchannels [6]. A PDMS wristband embedded with such a sensor capable of real-time pulse monitoring and a PDMS glove with multiple embedded sensors to provide comprehensive tactile feedback of a human hand when touching or holding objects were built.

A wide range of pressure sensors are based on electrical transduction mechanisms like piezoresistive, piezocapacitive, piezoelectric and triboelectric devices. It is not surprising since electrical output signals are easy to process, conditioning circuit are usually simpler and devices are cheaper to build and more adaptable. Piezoelectricity is the property of peculiar materials to gain a measurable voltage drop at their ends when stretched or compressed (direct piezoelectric effect) and, on the contrary, the application of an external voltage difference forces a mechanical deformation (reverse piezoelectricity) within the piezoelectric material. Pressure sensors exploit direct piezoelectric effect, converting mechanical stimuli into voltage differences. The mechanical-electrical conversion can be useful for energy harvesting. A lot of research is going on piezoelectric devices thanks to the dual possibility to harvest energy and sense mechanical stimuli. To name but one, "smart" fabrics are composed by a pressure-sensitive piezoelectric layer sandwiched between two conductive layers and infused into a flexible fabric which becomes capable of sense, monitor and harvest energy. These sensors are currently being developed for use as shoe insoles and clothing (website https://blog.piezo.com/piezoelectric-energy-harvesting-within-wearable-devices-summary).

Just like piezoelectricity, the triboelectric effect is another electric phenomenon suited for energy

harvesting application. It consists in the generation of a voltage difference between two different materials (one at least insulating) when rubbed one against each other, as a consequence of electrons transfer. Very well-known is the example of amber that if rubbed with a wool fabric is able to attract small pieces of paper. Triboelectric effect has earned popularity when in 2012 the Prof. Wang's group at Georgia Institute of Technology first demonstrated triboelectric nanogenerators (TENGs) as energy harvesting technology. The basic working principle of TENGs comprises the coupling of triboelectrification and electrostatic induction during the conversion of mechanical energy to electricity. Through the years several TENGs configurations have been proposed like the Vertical Contact-Separation Mode, Lateral Sliding Mode and Single-Electrode Mode. The advantages of the TENG include low cost, structural diversity and high energy conversion efficiency, and have led to rapid development of wearable and implantable solutions. Hearth rate, pulse, respiratory rates are examples of physiological body mechanical signals that can be read from wearable and implantable TENGs and, in addition, the electric power acquired from their conversion could feed low-energy electronics such as smartwatches [18].

Piezoresistive sensors work on the principle of converting applied pressure on the device into electrical resistance variation. In the work of Park et al. a shrink-film, a shape memory polymer that retracts upon heat, was used to transfer wrinkling in carbon nanotube thin films, which improves pressure sensitivity due to the higher surface roughness. The piezoresistive effect comes into play when two creased electrodes are coupled together and the number of electrical contact points changes upon actuation thereby changing the electrical resistivity. Mounting the sandwiched electrodes on a volunteer's throat and let him spoke various phrases was possible to successfully distinguish among different words, demonstrating potential voice detection applications [21].

Similarly, capacitive sensors transduce an applied pressure into electrical capacitance variation. In short, taking as reference a common parallel plate capacitor, the electrical capacitance formula reads:

$$C = \varepsilon_0 * \varepsilon_r \frac{A}{d} \qquad \text{(C formula)}$$

where ε_0 and ε_r are the vacuum and relative dielectric constants respectively, A is the faced area of the armatures and d their mutual distance. Assuming $\varepsilon = \varepsilon_0 * \varepsilon_r$ as fixed, wearable pressure sensors are expected to be at least stretchable, so that the application of pressure results into a geometry modification of the capacitor area A and the armature mutual distance d.

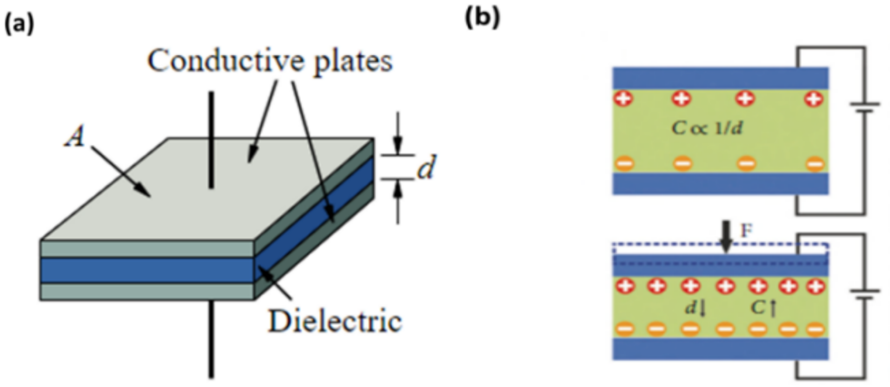

Figure 5 (a)parallel plate capacitor (b)the application of an external force reduces the plates distance, increasing the capacitance

As hinted in figure5, the applied pressure generates a proportional relative capacitance change which on its own is inversely proportional to distance variation, and can be measured inserting the stressed capacitor in an electric circuit. Indeed, both piezoresistive and piezocapacitive devices have the disadvantage to be constantly battery-powered in order to work, but they also benefits from lower manufacturing cost and simpler working principle than piezoelectric and triboelectric ones. Several electrode and dielectric materials, configuration and manufacturing techniques have been explored in literature.

3 Piezocapacitive pressure sensors

Capacitive pressure sensors have attracted more interest compared to other types of sensors such as resistive, piezoelectric and triboelectric, thanks to their simple structure, low fabrication cost, low power consumption, high sensitivity, good dynamic response performance and strong adaptability to harsh conditions such as high temperature, radiation and strong vibration [7][16]. According to the previously explained configuration and working principle of a capacitive pressure sensor it is straightforward that a highly deformable dielectric layer is the crucial component for enhancing the sensitivity [7]. Promising candidate for this task are the hydrogels, 3D crosslinked networks of hydrophilic polymers capable of retaining large volumes of water. They are either chemically or physically crosslinked and possess highly tunable structural and mechanical properties that can be tailored to the specific requirements of flexible pressure sensors [10]. Water evaporation is one of the main issue with hydrogels since they become dry and losses their physical properties, while the other great challenge with conductive hydrogels is to overcome the incompatibility between mechanical elasticity and high electrical conductivity [11].
Porous sponges made up of porous polymers are an interesting alternative to hydrogel. The porous structure lends flexibility, lightweight, the possibility to load huge amount of conductive filler without the risk to loose the physical and mechanical properties over time and, moreover, merges an high pressure sensitivity with a wide sensing range. In literature several preparation mechanisms of porous sponges for piezoresistive or capacitive pressure sensors have been studied and will be illustrated in the following.

3.1 Sugar based methods

One of the most cost-effective fabrication method is the sugar templating process, in which a commercial sugar cube acts as sacrificial template to realize the polymer sponge. Firstly, some liquid uncured polymer is prepared, Polydimethylsiloxane (PDMS) is one of the most commonly used elastomer materials thanks to its unique advantages, such as applicable temperature range (from $-100\,^{\circ}$C to $200\,^{\circ}$C) and chemical stability [8]. Secondly, either the sugar cube is soaked for around one third of its length in the liquid elastomer or the polymer is gently poured on it, while a surrounding vacuum pumping system helps the liquid paste to fully impregnate the sugar cube. The filled cube is put in a oven to cure the elastomer. After curing, the sugar is dissolved by immersion in deionized (DI) water leaving the polymeric sponge to inherit the aspect ratio of the pristine sugar cube and average pores size equals to the dimensions of the sugar crystals composing the template cube. Finally, the sponge is rinsed in DI water to remove sugar residuals and dried in a oven or in ambient conditions for a longer time. Using the sugar templating method Iglio et al. realized a PDMS foam decorated with pristine multiwalled carbon nanotubes (CNTs) [8]. Decoration with CNTs is carried out by drop-casting of a number of drops (0.8 mL each) of a CNTs ink on top of the PDMS foam. The CNT ink consists of a dispersion of pristine CNTs in ethanol and its evaporation at ambient temperature results in the physical absorption of CNTs on the inner pore surfaces of the foam via physical interaction, conferring a superior electrical conductivity. The main drawback in decoration of bare PDMS foams with CNTs is the worsening of mechanical flexibility of the sponge. To further enhance the overall performance of pressure detection, Zhao et al. used a PDMS sponge as flexible matrix and three conductive fillers composed of zero-dimensional Ag

nanoparticles (NPs), one-dimensional CNTs and two-dimensional graphene [27]. The ameliorated sensitivity and stretchability are attributed respectively to the increased conductivity of Ag-CNTs-graphene composites by electron transferring from Ag NPs to CNTs and graphene, and to better flexible stability of the CNTs-graphene matrix.
The use of commercial sugar cubes as template strictly fixes the shape of the polymer sponge to be cubic itself and this could limit the range of possible wearable applications. In the sugar molding methods is possible to overcome this restriction. Indeed, researchers developed some tecniques to realize an home-made sugar template of whatever desired shape. Jung et al. fabricated a porous CNT-PDMS composite structure (CPCS) by mixing in a beaker sugar powder, DI water and CNTs at a weight ratio of 30:1:0.01-0.3 (the CNTs concentration was varied to investigate the impact over electrical conductivity and mechanical properties) [9]. The mixture was placed in cases of desidered shapes and after 4 h of water evaporation at room temperature (RT) sugar grains stuck together replicating the molds aspect, as shown in fig. 6. The customized sugar template was then exploited as in the ”standard” sugar templating method.

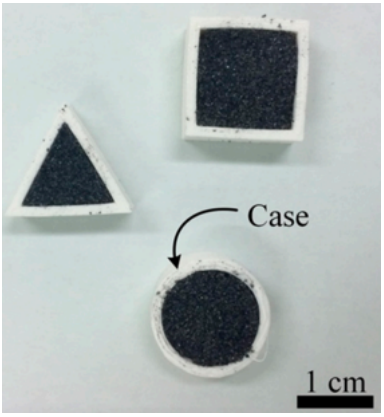

Figure 6 Cases used to shape sugar cubes incorporated with CNTs

Alternatively, PDMS can be directly mixed with screened sugar particles in the mold. The screening is needed in order to finely tune the final pore size in the sponge. Using a vacuum desiccator, like in the work of Li et al. [16], the original air in the gap of sugar particles would be evacuated, and the liquid of PDMS wuold be vacuum-assisted compressed into these air voids. After fully filling, the porous PDMS could be obtained by demolding and immersing into DI water to dissolve the sugar particles away. Sugar particles are chosen as porogens thanks to their excellent mechanical stability [23], but also salt is a valid candidate. Dan et al. compared potassium chloride (KCl) and NaCl with sugar particles to find the best sacrificial powder template for their device [3]. They realized a resistive pressure sensor with a sandwich structure composed of top and bottom sheets of porous PDMS fabricated by using the template method. The inner face of each of these layers is coated with a layer of conductive Ag nanowires (NWs). The study of the impact of different pore size on device performance highlighted that the sensors fabricated with KCl porous layer (which had the smallest pores) had the best performance.

3.2 Emulsion

Sugar and salt are solid powder templates and the size of their particles strictly fixes the dimensions and shape of the pore in the polymer foams. Liquid templates could overcome this limit and

emulsions are common examples. The average droplet size and distribution is tunable by varying the emulsion composition and, after the polymerization of these emulsions, the pores of the final polymer foams inherit the shape of the droplets of the emulsions [22][2]. A general emulsion process is showed in figure7. An emulsion template is created by mixing two non miscible liquid phases like water and oil. The oil phase is a monomer phase and it is usually reffered to as continuos phase while the acqueous phase, or internal phase, is dropwise added into the former. By keeping the solution under continuos stirring, the feeding of the acqueous phase results in a stable emulsion of water droplets within the monomer phase that is called High Internal Phase Emulsion (HIPE). Subsequently, the emulsion is put in a oven to polymerize the monomer phase which becomes a Polymerized HIPE (polyHIPE). The simultaneous water evaporation results in empty pore dispersed into a solid polymer matrix that is the final polymer foam. In order to enhance the stability of the emulsion and the electrical conductivity of the final foams, water droplets could be loaded with surfactants agents and conductive particles that will stick in the inner pore surfaces of the foam during the oven step. Yang et al. investigated the impact of pore structure on the mechanical, electrical and piezoresistive properties of the developed foams by tuning the droplet size distribution of the emulsion, which was regulated by changing the pH and conductive graphene oxide (GO) loadings [25]. Superior performances such as higher pressure sensitivity and wider pressure responsive range were obtained through the pH-GO combination which led to the formation of both broad and small pores in the polymer foam, i.e. a hierarchically porous foam.

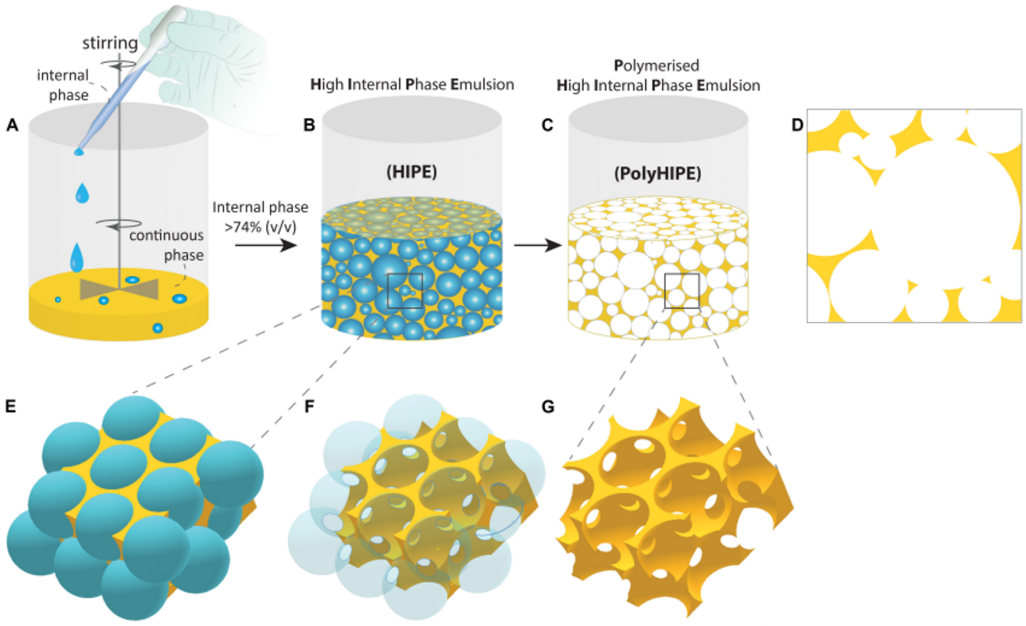

Figure 7 Common steps of an emulsion templating process. Figures from E to G highlight the water droplets inclusion in the monomer phase, their evaporation and consequent creation of a porous polymer sponge, respectively.

3.3 Exotic synthesis methods

Beside templating fabrication methods, literature is plenty of unique and creative alternatives. For example, researchers adopted commercially available elastic foams with regular structures such as polyurethane (PU) and melamine sponges to develop pressure sensors by construction of conductive networks on their skeletons. Main drawbacks of commercial sponges are short working range and small linear responsive region. Dong et al. found in biomass sea sponge the chance to extend the range of linearity of piezoresistive pressure sensors [5]. Sea sponge (Phylum Porifera, fig8a) offers on its own an intrinsic hierarchic porous soft structure composed by triangle nodes size distributed in the range 200-900 um (fig8c), never seen in standard commercial sponges. A virtual reconstruction of the porous matrix of the sponge can be seen in the figure8b. Moreover, a composites conductive networks of reduced GO and Ag NWs were added through the dip-drying method (immersion into GO or Ag NWs suspension followed by drying at RT). The synergy between hierarchic porous structure and composites conductive networks linearized the pressure sensitivity over an extraordinary wide sensitive range (0-40 kPa).

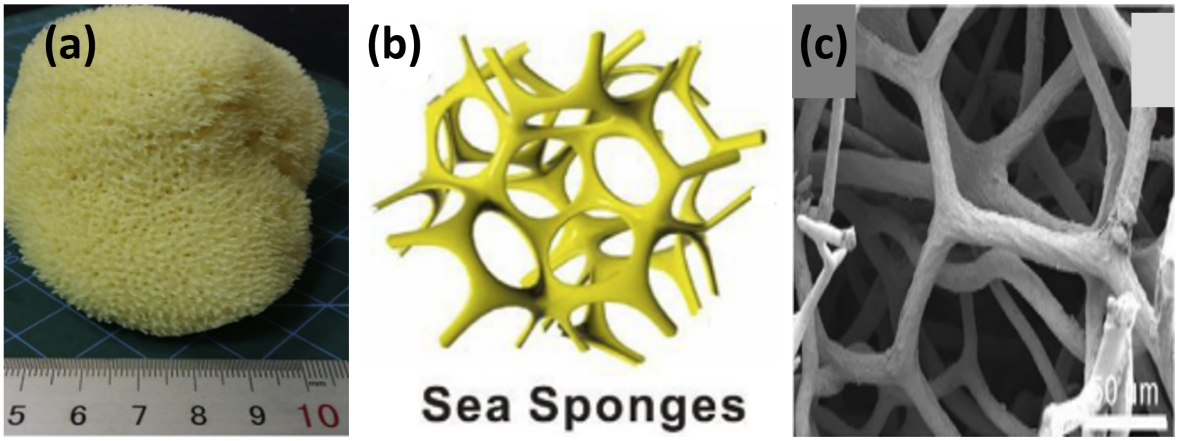

Figure 8 (a)Phylum Porifera sea sponge (b)model of the sponge porous matrix (c)Scanning Electron Microscope (SEM) image of the Phylum Porifera

Templated, commercial and natural foams are all afflicted by great variability in the pores size which on one side improves the sensing performance of the single sensor but on the other side negatively weighs over sensor-to-sensor uniformity. It is totally unpractical to build an array of sensors if they have so largely varying characteristics. Oh et al. promoted to solve the issue by means of a microfluidic emulsion droplet self-assembly technique , which generates highly reproducible and uniformly sized pores assembled in a highly ordered close-packed manner [20]. Using a T-junction microfluidic channel (fig9), uniformly sized water droplets were injected into a mold containing an oil solution consisting of precured PDMS and droplets stabilizing agent. Water droplets were denser than the oil solution so they sank to the bottom of the mold. The emulsion was then heated in an oven, where the water slowly evaporated and the PDMS cured, resulting in the highly ordered close-packed porous structure. To fabricate a piezoresistive pressure sensor the surface of porous PDMS was chemically grafted with polypyrrole (PPy, a conductive polymer). This ensured a strong covalent bonding between PPy and PDMS as opposed to weak physical adsorption of conductive

fillers (such as AgNWs, CNT, GO, graphene and so on), favouring a positive reduction of hysteresis, the difference in the sensor output signal under loading and unloading of pressure, which causes inaccuracy in measurement.

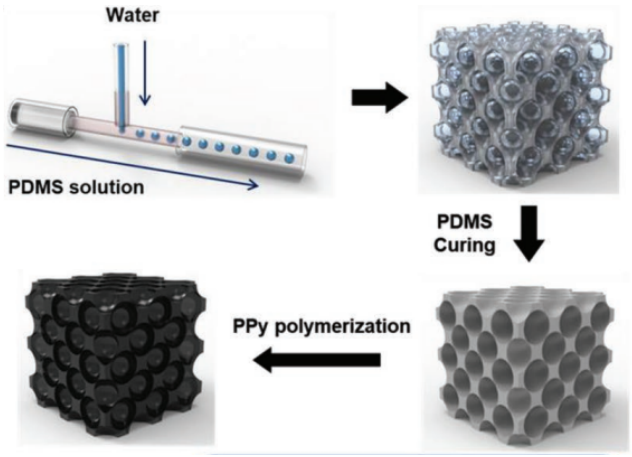

Figure 9 Main steps of the microfluidic emulsion droplet self-assembly technique

Finally, a summary table with a comparison among samples produced with different method is reported.

Ref	Fabrication	Materials	MAX S, kPa^{-1}	$\Delta R/R_0$, $\Delta C/C_0$	LOD, Pa	Working Range, kPa
18	Sugar Powder	PDMS, AgNWs	0.62	-	-	-
19	Sugar Cube	PDMS, CNTs	0.9	≈ 15	6	50
20	Sugar Cube	PDMS, Ag NPs, CNTs, graphene	33	95	-	-
21	Sugar Powder	PDMS, CNTs	0.015	≈ 70	-	50
22	KCl Powder	PDMS, AgNWs	14.1	≈ 80	-	40
23	Emulsion	Monomers, GO	0.83	-	-	>200
24	Sea Sponge	AgNws, GO	0.016	50	0.28	40
25	T-junction	PDMS, PPy	0.07	≈ 90	80	100

4 Sensor preparation

Herein, a porous PDMS-based sponge for capacitive pressure sensing is realized. Polydimethylsiloxane (PDMS) is a silicon-based organic polymer composed of a repeating unit $SiO(CH_3)_2$ (fig.10a). It founds many applications in various field ranging from engineering to cosmetics thanks to low cost, non-toxicity, good elasticity and high flexibility, thermal and chemical stability. PDMS is a two-component polymer, a viscous base elastomer and a liquid curing agent (or cross-linker). Only once mixed, the curing agent cross-links the elastomer chains allowing the base elastomer to pass from viscous to elastic solid phase, similar to rubber. The curing or polymerization process requires 24h at room temperature and it's sped up by heating. The final mechanical properties of the cured PDMS depend on the exact ratio between base elastomer and curing agent and on curing temperature. For this work the two component kit of Sylgard@184 monomer and curing agent were purchased from Dow Corning Corporation (fig. 10b).

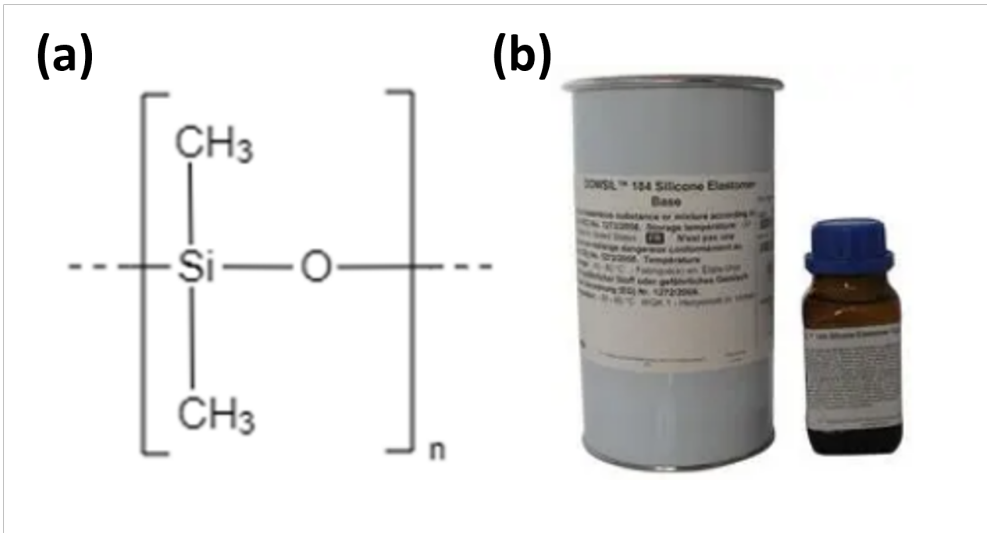

Figure 10 (a)PDMS repeating unit (b)PDMS components kit (Sylgard@184): base elastomer on the left and curing agent on the right

The synthesis process of the porous PDMS foam was based on the use of commercial sugar, both in the form of cube to act as a template and in the form of a common powder to prepare samples by casting in a mold. The two fabrication methods are presented below.

4.1 Sugar Templating Method

Herein, the main fabrication steps are listed.

1. Base elastomer and curing agent are mixed in the desired ratio in a baker and are manually stirred with a metallic spatula for 2 minute. The base elastomer to curing agent ratio is expressed as X:1 were is X = {5,10}, and the corresponding sponge is from now on called X:1 sponge, for the sake of brevity.

2. The stirring certainly incorporates unwanted air bubbles in the mixture so the baker is put in the vacuum gas pump for 15 min to degas.

3. At this stage a commercially available lump of sugar is soaked by half in the degassed blend and degassed in the vacuum pump for 15 min to help the liquid PDMS to totally fill the inner pores of the sugar cube. The process is repeated for the other half of the cube. The figure 11 shows the sugar cubes during the vacuum-assisted PDMS infiltration.

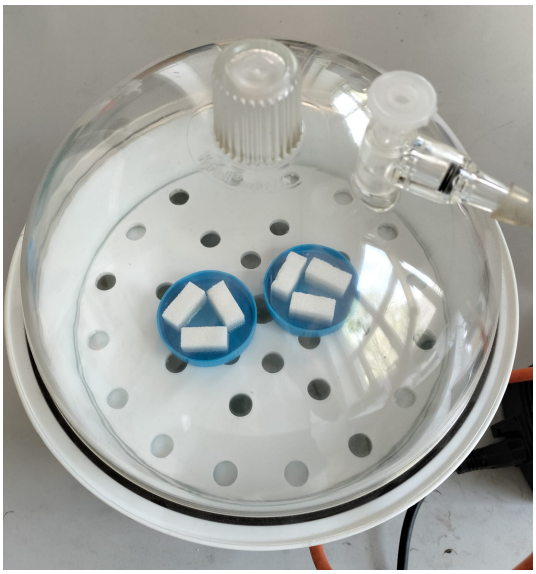

Figure 11 Some lumps of sugar half soaked in PDMS inside the vacuum gas pump

4. The infiltrated sugar cube is firstly cleansed by the excess of unabsorbed PDMS with a paper and secondly is inserted into the oven (Memmert) at 60°C for 1 hour to cure the PDMS.

5. After curing, the cube is submerged in a baker full of DI water in order to dissolve the sugar template. The water is kept in constant agitation and at almost 60°C for 30 min by a magnetic stirrer. The complete dissolution of sugar template results in a porous PDMS (pPDMS) foam with pore sizes comparable to those of the sugar grains of the template [8].

6. The as-prepared pPDMS is washed a couple of time with DI water and dried into the oven at 60°C.

The listed steps are summarized in figure 12a together with a sketch of the PDMS infiltration within the sugar cube voids among the inner sugar crystals (fig12b).

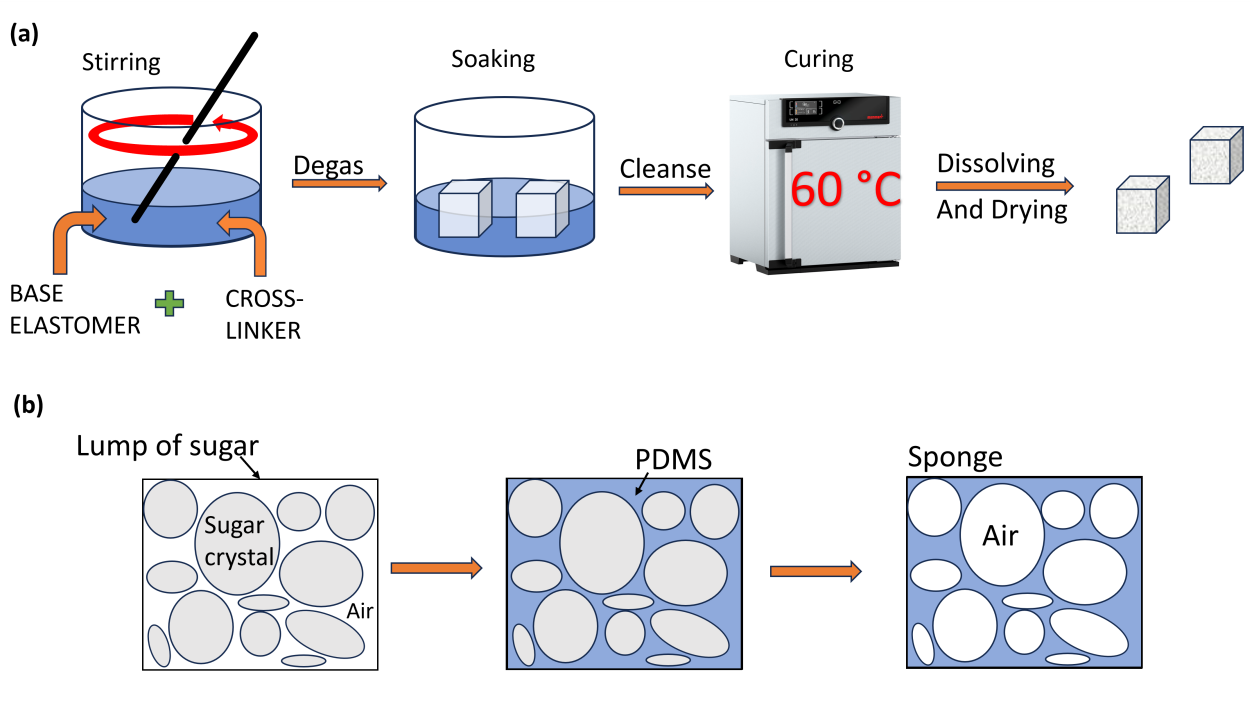

Figure 12 (a)templating method main steps (b)skect of PDMS infiltration in the sugar cube

4.2 Sugar Molding Methods

With the aim of disregard the shape of the sponge from that of the cubic sugar template two alternative sugar molding approaches were used.

4.2.1 PDMS and sugar mix

The uncured PDMS and the sugar powder were directly mixed together to be poured in a case. First of all, base elastomer and curing agent were mixed in the desired ratio and degassed. Later, a commercial soft white sugar was added in a 3:1 or 4:1 ratio with respect to the uncured PDMS. The paste was vigorously stirred by hand for a couple of minutes to reach a sufficient degree of homogeneity and to avoid PDMS sediment. Thereafter, the mixture was poured on a mold, compacted, and cured in the oven at 60 °C for 2 hour. After the curing process, the sugar was washed away through a DI water bath in a magnetic stirrer (60 °C, 30 min) and the resulting molded porous foam was washed and dried. The main steps are summarized in figure 13.

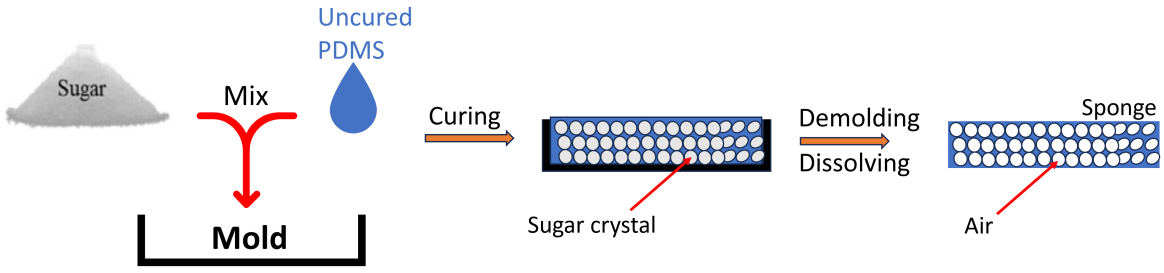

Figure 13 Molding method main preparation steps

4.2.2 Homemade sugar cube

Alternatively, a lump of sugar can be simply made with water and powdered sugar. A commercial soft white sugar was mixed with DI water at a weight ratio of 30:1, and placed in a case of desired shape. By evaporating the water for 4 h at room temperature, some parts of the sugar grains stuck together and connected to form a sugar cube [9]. The sugar cube was separated from the mold and ready to be subjected to steps from 3 to 6 of the list above.

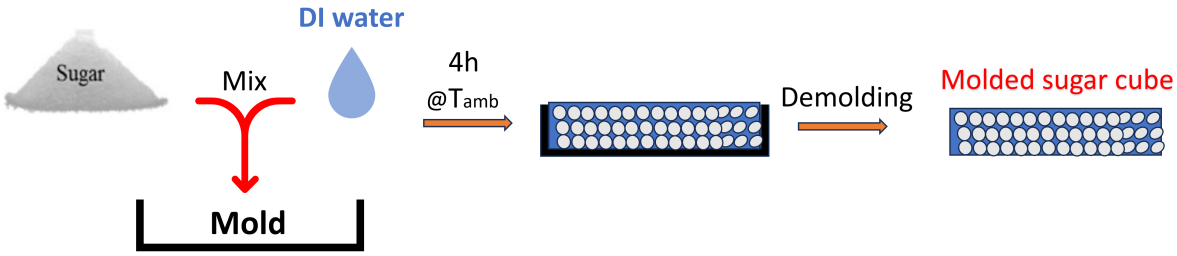

Figure 14 Homemade sugar cube main preparation steps

4.3 Addition of conductive nanofillers

In this section the tecniques used to ameliorate the electrical properties of the sponges are explained. Indeed, pPDMS sponges are characterized by good flexibility and stretchability but suffer from poor electrical conductivity, which is a fundamental parameter in wearable electronics. Conductive polymer composites (CPCs) are simply fabricated by adding conductive nano-fillers (such as metal nanoparticles, carbon nanotubes and nanowires, graphene nano-sheets, etc.) to the polymer matrix through various processing methods. The large porosity of polymer sponges enables them to host high loadings of conductive fillers, boosting the electrical behaviour.
In this work, two decoration methods were investigated:

1. immersion of a ready-made sponge in a liquid solution containing a metal precursor
2. a priori addition of a conductive powder or a metal precursor solution together with the base elastomer and the curing agent before the PDMS curing phase (then, followed steps from 2 to 6 of the previous list)

The metal precursor solutions were adopted as conductive ingredients since the curing agent is able to reduce the precursors forming metal nanoparticles that will incorporate in the future sponge. In the immersion case the idea was to exploit the minimum residual amount of curing agent stuck over the inner pore surfaces of a ready-made sponge to directly synthesize metal NPs there. The metal precursor tried were Silver Nitrate ($AgNO_3$), Copper Acetate ($CuOAc$) and Iron Nitrate ($FeNO_3$), and the molar concentration was set equal to 40 mMol. In each solution were submerged for a whole night both a 10:1 and a 5:1 sponge. The experimental setup is shown in figure 15.

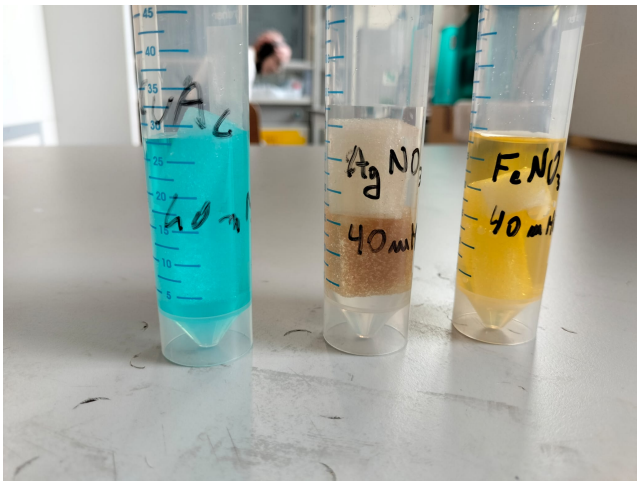

Figure 15 Solution of $CuOAc$ (blue), $AgNO_3$ (brown) and $FeNO_3$ (yellow) with ready-made sponges immersed

A stable change in color of the submerged sponge was assumed to prove for the metal NPs formation. As soon as the sponges were extracted from the solutions, they were colored, but after washing in DI water the samples with copper and iron turned white again, meaning that the metal NPs were actually not formed. Just the samples dipped in silver nitrate preserved the brown color (figure 16).

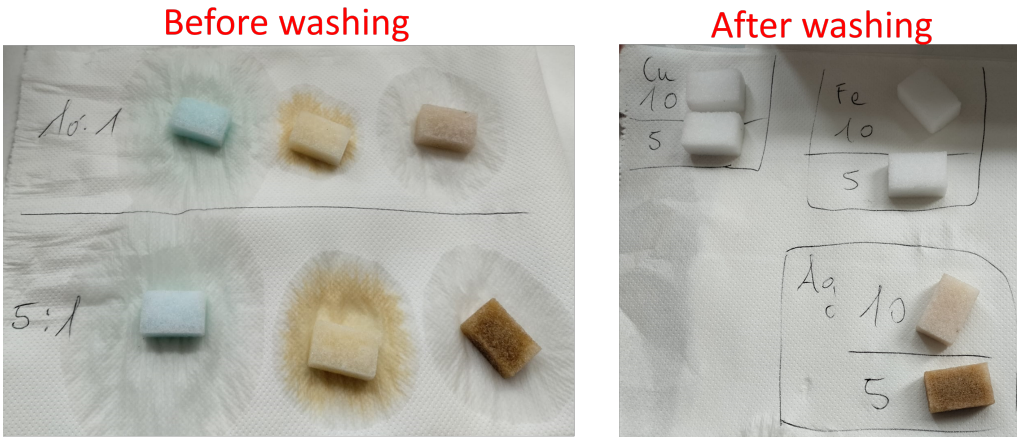

Figure 16 On the left there are the 10:1 (above) and 5:1 (below) sponges before rinsing, while on the right after rinsing

The metal precursor solutions were also a priori added to the uncured PDMS (fig17a) to benefit from the higher amount of curing agent and, if possible, a greater concentration of synthetized metal

NPs. The resulting mixture was magnetically stirred for 1 h (fig17b). Several PDMS quantities, stirring temperatures and molar concentrations were investigated.

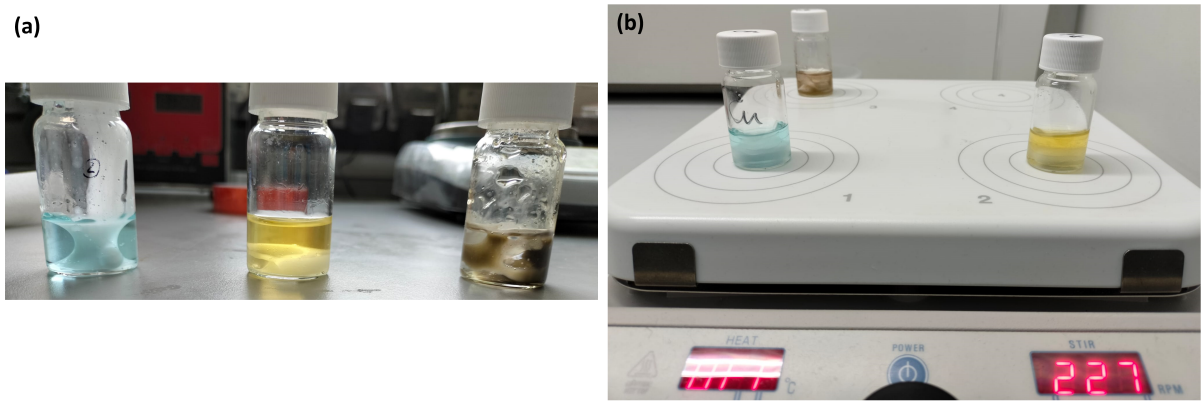

Figure 17 (a)bakers filled with uncured PDMS and $CuOAc$ (left), $FeNO_3$ (centre) and $AgNO_3$ (right), (b)bakers on the magnetic stirrer

Again, only the silver samples changed color steadily, even after the rinsing phase.
As an alternative to metal solutions, conductive nanofillers directly available in the form of powders, without the need to be synthetized from a precursor, were exploited too. The powder was added to the uncured PDMS and manually stirred for 2 minute with a metallic spatula. Powders of silver nanoparticles (Ag NPs), silver nanoflakes (Ag nFl) and carbon (C) mesoporous nanoparticles were used, and some characteristics are given in the table below.

Material	Shape	Average size, μm	Meso to micropore volume ratio	Molecular weight, g/mol
Silver	Flake	4 - 8	-	107.87
Carbon	Mesoporous particle	2 - 12	$>$1.6	12.01

Even though the common aim of all these functionalization tecniques was the reduction of the PDMS electrical resistance, they have all been failures in this respect. Nevertheless, they contributed at the significant increase of the sponge relative dielectric constant ε_r (C formula) with a consequent strong increase of the relative change in capacitance in response to the application of external pressure, improving sensor performance.

4.4 Sensor packaging

In order to compare the performances of sponges with different conductive fillers and preparation methods they were electrically and mechanically characterized. To this end, an equal package for all the sponges was designed. First of all, the pristine sponge was cut to scale the dimensions down to 3-5 *mm* of width and 140-200 mm^2 of surface area. A slide was cropped with a cutter in a rectangular shape to obtain two rigid planar supports on top and bottom of the sponge. Each of them was stuck with a common double-sided tape to an electrode, a Kapton foil overlapped to a copper one. The copper-side of the electrode was kept in close physical contact with the sponge by wrapping the whole package with some parafilm. Each portion of the electrodes coming outside of the parafilm was fixed to an electrical wire using a Kapton tape. An example of the final result is shown in figure 18.

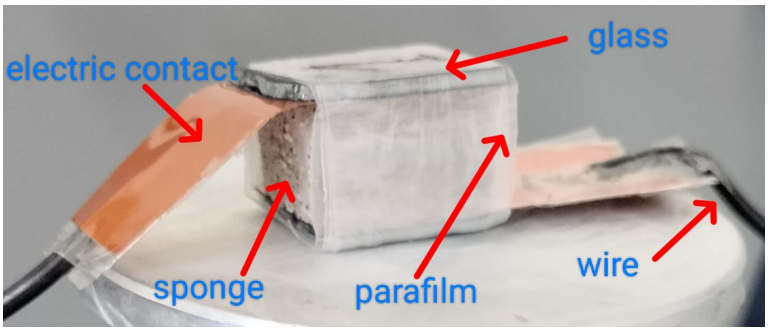

Figure 18 Sensor package

5 Characterization methods

All the sensors were subjected to mechanical stimuli, both in static and dynamic mode. The former required the use of calibration weights, while the latter an Instron tensile machine. During both kind of mechanical tests the change in electrical capacity under external deformation was monitored through an LCR meter (BK Precision 894). Parameter settings and data collection were assisted by LabView (National Instruments).
The capacitance measurement requires to apply an AC signal through the LCR to the sample, so first of all the values of voltage and frequency ensuring the lower possible noise were found. the reference sample was a bare pPDMS sponge provided with copper electrical contacts. A parallel between a resistor and a capacitor was used as model of impedance. the trials were performed by fixing the peak voltage value of the AC signal respectively at 0.5V, 1V and 2V, and by spanning the frequency from 1kHz to 500kHz. the sample was at rest, without any load applied, and the acquisition time of each trial lasted some seconds to collect enough stats. For each frequency-voltage pair, the mean and standard deviation of the relative acquisition were calculated and then compared. the measure with the lowest error was carried out at 300kHz and 0.5V so these were the testing electrical parameters used for all the successive studies.

5.1 Static Mechanical Tests

The static tests required the use of six calibration weights (1, 2, 5, 10, 20 and 50 grams) in the following way. Each of them was laid on top of the sensor and left a few seconds to allow the LCR to acquire a measurement range and successively evaluate the average capacitance at X gram of weight, $\overline{C_{Xg}}$, and the standard deviation, ΔC_{Xg}. The same approach was used to measure the resting capacitance C_0 of the sample, when no load is applied. Then, the relative percentage variation of the capacitance under static load was estimated from the formula:

$$\varepsilon_{Xg} = \frac{\Delta C_{Xg}}{\overline{C_{Xg}}} * 100 \tag{1}$$

The whole procedure was repeated five times and ε_{Xg} was averaged among the five acquisition, at same weight. For the general X weight the calculus reads:

$$\overline{\varepsilon_{Xg}} = \frac{\varepsilon_{Xg}^{1^{st}acq} + \varepsilon_{Xg}^{2^{nd}acq} + \varepsilon_{Xg}^{3^{rd}acq} + \varepsilon_{Xg}^{4^{th}acq} + \varepsilon_{Xg}^{5^{th}acq}}{5} \tag{2}$$

At this point, the uncertainty about $\overline{\varepsilon_{Xg}}$ was evaluated by the half maximum deviation, according to the formula:

$$\delta C_{Xg} = \frac{\varepsilon_{Xg}^{MAX} - \varepsilon_{Xg}^{MIN}}{2} \tag{3}$$

where ε_{Xg}^{MAX} and ε_{Xg}^{MIN} are respectively the maximum and the minimum relative variations among the five acquisitions, at the same X weight. Then, the quantities $\overline{\varepsilon_{Xg}} \pm \delta C_{Xg}$ were plotted against the six weights in an error bar plot. The slope of linear fit between 0 g and 5 g represented the static sensitivity (SS) of the device, defined as the relative percentage change in capacity for each gram of load. As an example, in figure 19 it is shown the error bar plot of the pPDMS sponge with a base-curing ratio of 5:1.

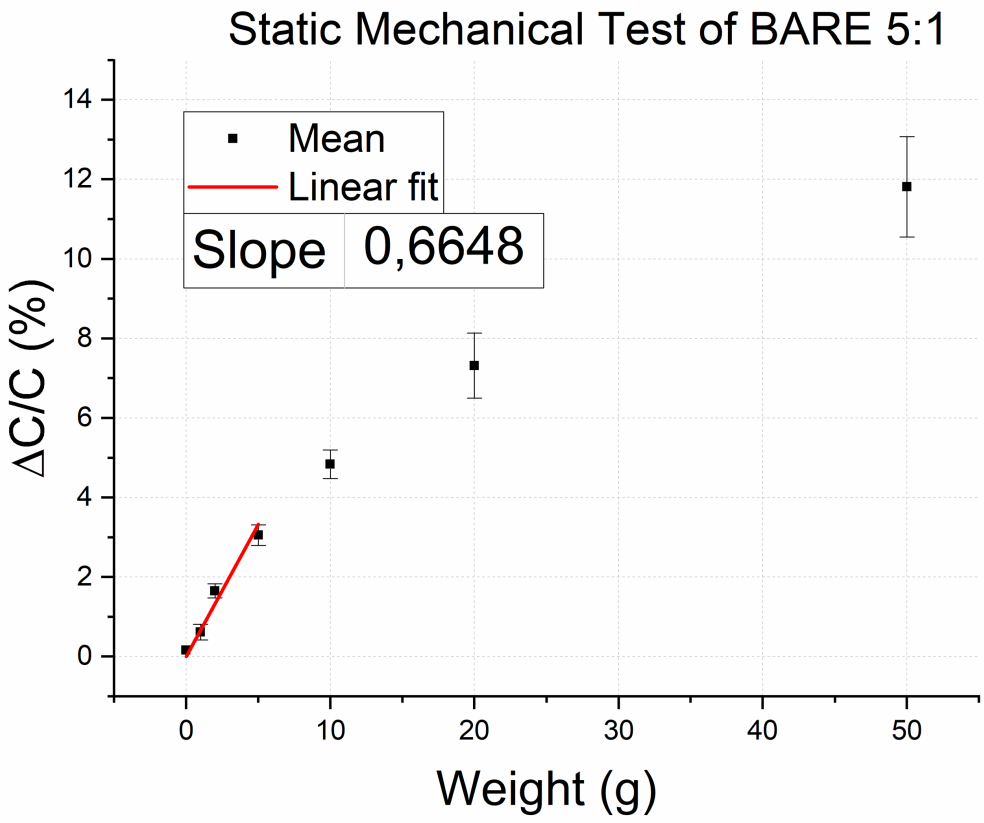

Figure 19 Average relative percentage change in capacity versus the weights in grams. The slope of the linear fit (red line) is the static sensitivity.

At this stage, it was possible to evaluate the Limit Of Detection (LOD) of the device, that is the minimum weight that can be sensed with a sufficient degree of confidence. The LOD is calculated by the formula:

$$LOD = \frac{3 * \overline{\varepsilon_{0g}}}{SS} \tag{4}$$

In other words, the more accurate the estimation of the resting capacitance (lower standard deviation), the lower the minimum weight or pressure that can be detected by the device. An example of LOD measurement is shown in the zoom (20) of the figure above (19).

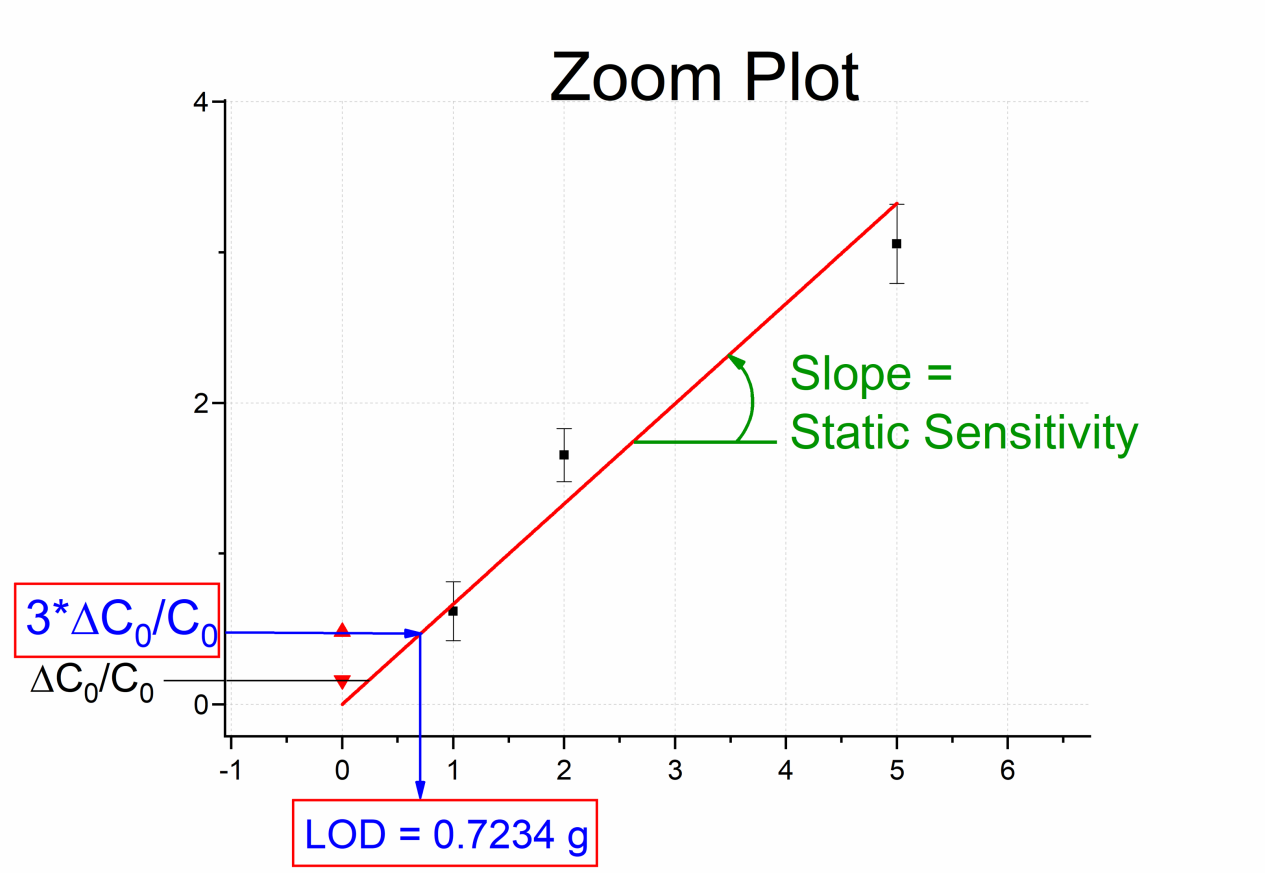

Figure 20 Zoom of figure 19 showing the LOD evaluation.

5.2 Dynamic Mechanical Tests

An Instron tensile machine with a load cell of 500 N was used to compress the sensor, both in single runs and in a cyclical manner. The Instron parameters setting was assisted by the software BlueHill. The change in capacity was simultaneously recorded by the LCR meter connected to the electrical wires of the sensor under test. The whole test bench is shown in figure 21a.

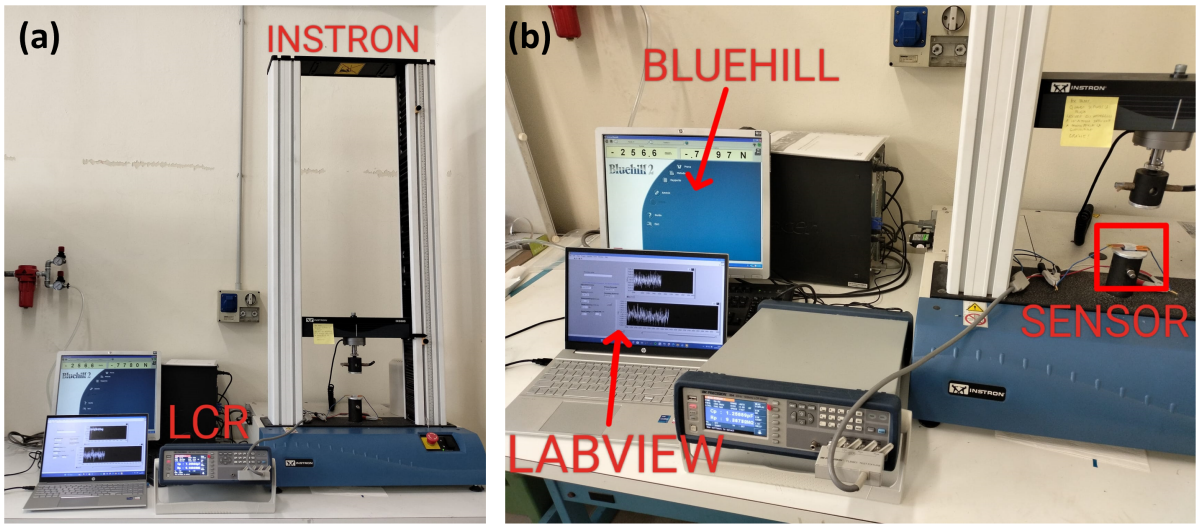

Figure 21 (a)whole dynamic test bench (b)zoom around the sensor and the instrumentations

5.2.1 Single Run Test

In a single run measurement the sample is squeezed from zero up to a maximum value of applied force, with a certain velocity. The zero of the force did not exactly coincide with 0 N since an initial pre-load of 50 mN was necessary to flatten the package of the sensor and ensure a good electrical contact. The maximum load was fixed to 50 N while the compression speed was varied to study the impact over the deformability of the sponge. So, assuming the spatial position of the upper piston in correspondence of the applied pre-load to be at coordinate zero of an imaginary x-axis, the Instron recorded the change in time of the applied force up to 50 N and the change in time of the piston deviation from the initial reference position, in millimeters. In the meanwhile, the LCR monitored the change over time of the capacitance. From the mechanical measurements were extracted on one hand the relative percentage change of the sponge width, also called strain, according to:

$$\varepsilon_{\%} = \frac{\Delta l(t) - l_0}{l_0} * 100 \tag{5}$$

where $\Delta l(t)$ is the time deviation of the piston and l_0 is the resting sponge width, and on the other hand the pressure time change $\sigma(t)$, measured in kPa and called stress, dividing the applied force by the sensor area. From the electrical measures was obtained instead the relative percentage change in capacity, defined as:

$$\frac{\Delta C}{C}(t) = \frac{C(t) - C_0}{C_0} \tag{6}$$

where $C(t)$ and C_0 are respectively the capacity at a certain applied pressure (or force) at time t and in correspondence of the applied pre-load at time t =0 s. The dynamic sensitivity of the device was obtained from the linear fit of the plot of $\frac{\Delta C}{C}(t)$ versus $\sigma(t)$, and it represents the relative change in capacity in correspondence of a unit pressure variation, within a certain pressure range. An example is shown in figure 22.

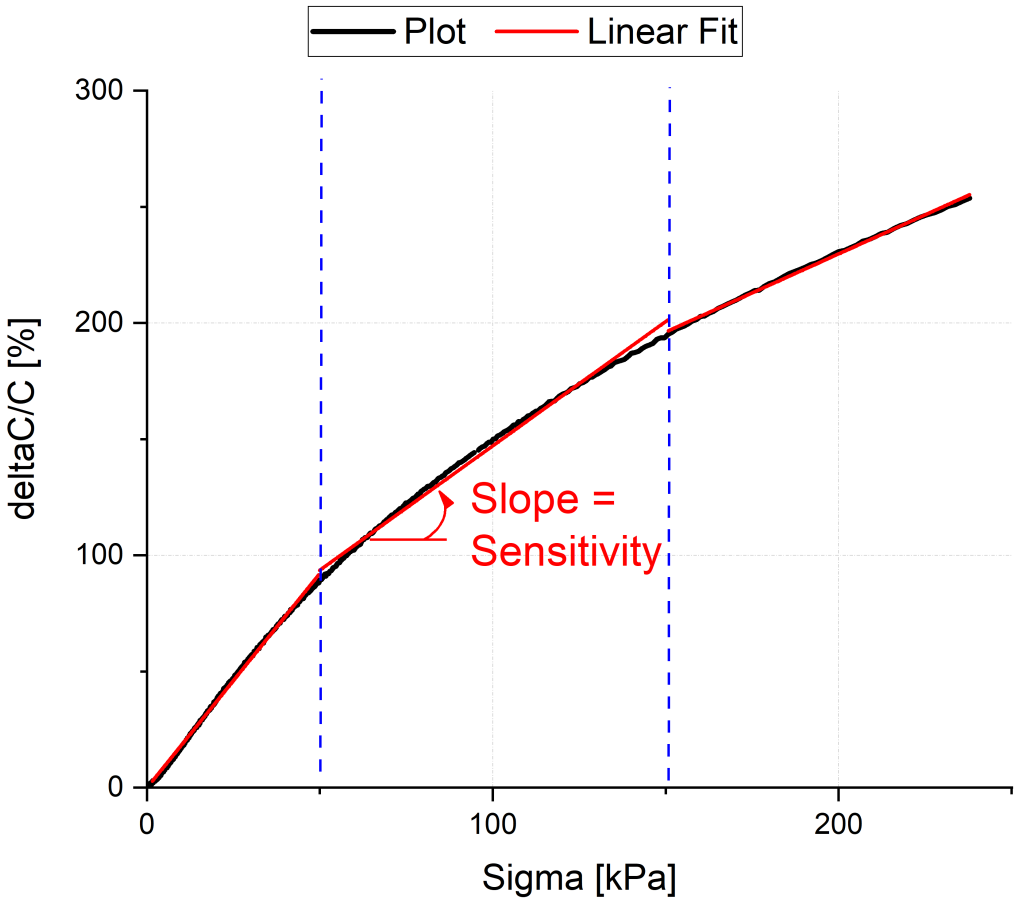

Figure 22 Example of dynamic sensitivity determination.

In general, the sensitivity lowers along the pressure sensing range. Another interesting quantity to describe is the stiffness of the sponge, and it is linked to the plot of the pressure $\sigma(t)$ versus the relative width change $\varepsilon = \varepsilon_{\%}/100$, also called stress-strain curve. It describes the relative deformation of the sponge width for a certain applied pressure. The slope of the linear fit of the very first part of the curve is the Young's Modulus that is a measure of the stiffness of the sponge (fig23). The higher the Young's Modulus, the softer the sponge.

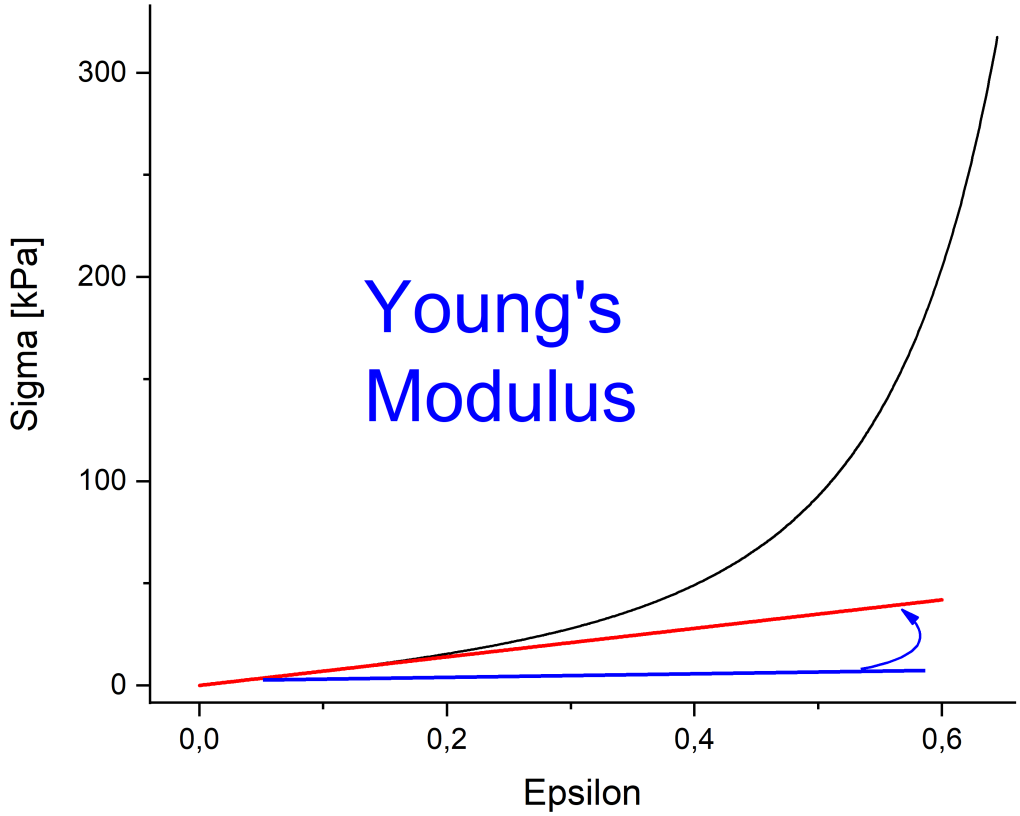

Figure 23 An example of Young's Modulus determination. The red line is the linear fit of the black curve.

5.2.2 Cyclic Test

In the cyclic mechanical test the compression force of the piston varied from the pre-load value to the maximum one and then the other way around, for a certain number of times. Even in this case different compression velocities were compared. The cyclic tests are useful to study the stability of the electrical response of the device during repeated application of a load. Moreover, the area within the stress-strain (σ-ε) graph is proportional to the hysteresis of the device.

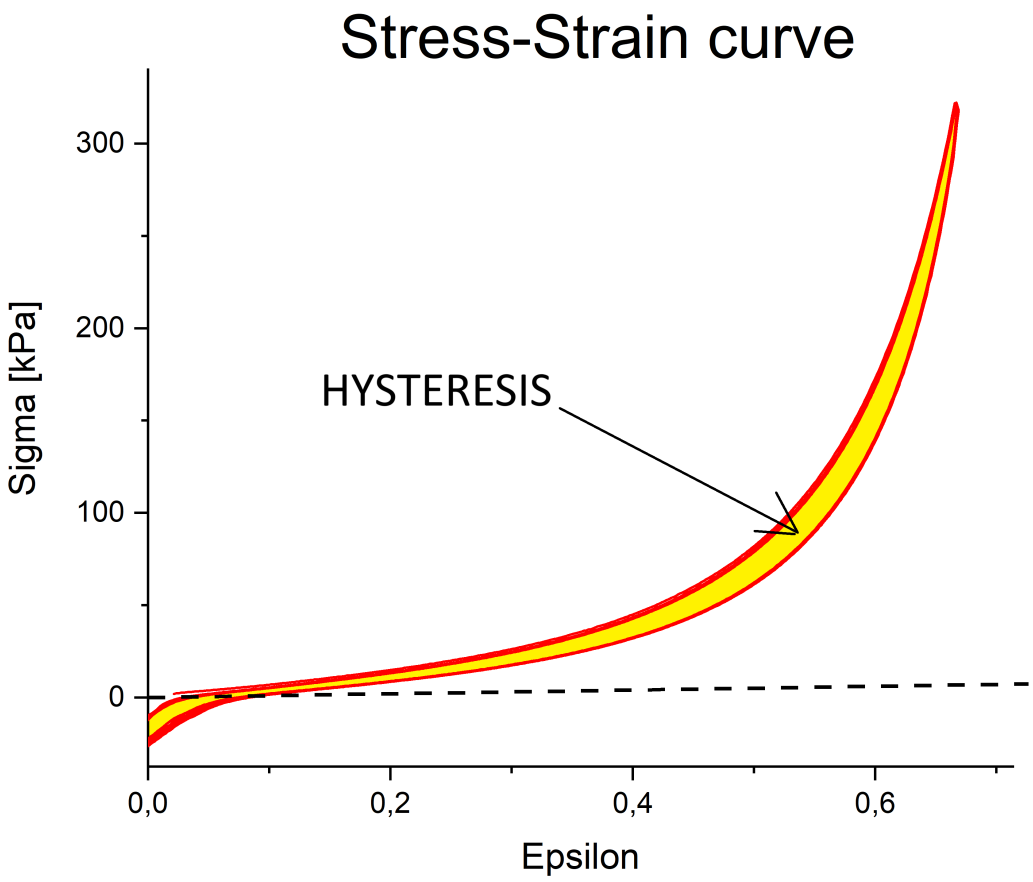

Figure 24 The colored area of the σ-ε is proportional to the hysteresis of the device.

6 Results: template sensors

The results discussion is separated in two macro sections according to the sponge fabrication method: the sugar templating, or the sugar molding, as presented in the Materials and Methods chapter. Within each section there is a further distinction based on the way the foams are decorated with conductive nano-fillers, or left as they are. Moreover, the main physical quantities characterizing the performance of the devices are compared to evaluate the most sensitive device. In the followings, the template samples are presented.

6.1 Bare pPDMS sponges

Herein, bare sponges without any conductive nanofillers are presented. First of all, a check on the variability of the sponge deformability according to the compression speed was done. The 5:1 sponge is taken as a reference to show the results. It was compressed in a single run from 50 mN to 50 N with three different speeds, 2 mm/min, 5 mm/min and 10 mm/min. The σ-ε plot in figure 25a shows three almost coincident curves, underlining a negligible viscoelastic effect. Also the electrical properties are almost unvaried, as evidenced by the substantial coincidence of the capacitance change

with respect to stress σ and strain ε (fig25b-c).

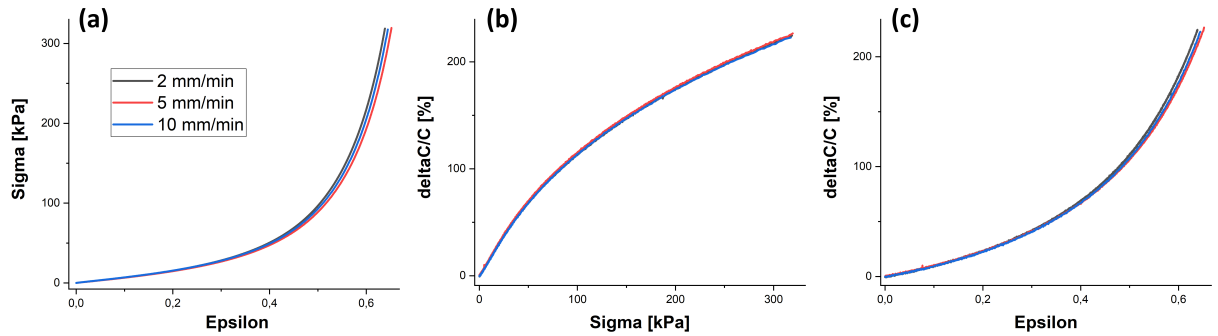

Figure 25 Single run compressions at 2 mm/min, 5 mm/min and 10 mm/min compression speeds of the 5:1 bare sponge: (a)stress-strain curve, relative change in capacitance with respect to (b)stress and (c)strain

The same discussion applies for cyclic tests too, in which the sample was subjected to 10 compression cycles at 10 mm/min and 20 mm/min in figure 26.

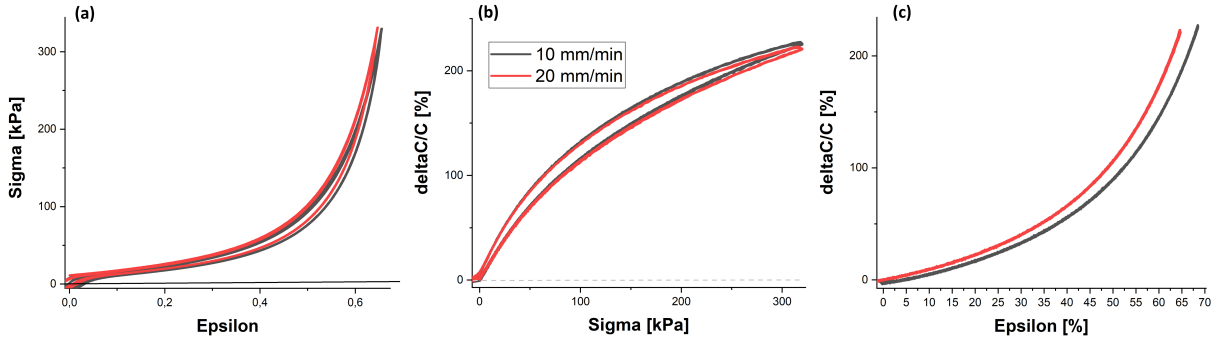

Figure 26 Bare 5:1 sponge cycle tests: capacity change with respect to (a)stress and (b)strain, and (c)stress-strain curves at 10 mm/min and 20 mm/min compression speeds

In light of these observations the successive measurements for all the other samples were carried out at a compression speed equal to 10 mm/min for the single run and of 20 mm/min for the cycles, because the results of the tests were identical to those conducted at lower speeds but with the advantage of a faster measurement. The number of cycles was fixed to 10.
Now, the results of the comparison between a 5:1 and a 10:1 bare sponge are presented in figure 27. The samples show almost the same variation in capacity depending on external pressure (27a). A slight difference in the mechanical properties is visible in figure 27b where the 10:1 sponge undergoes a higher percentage deformation.

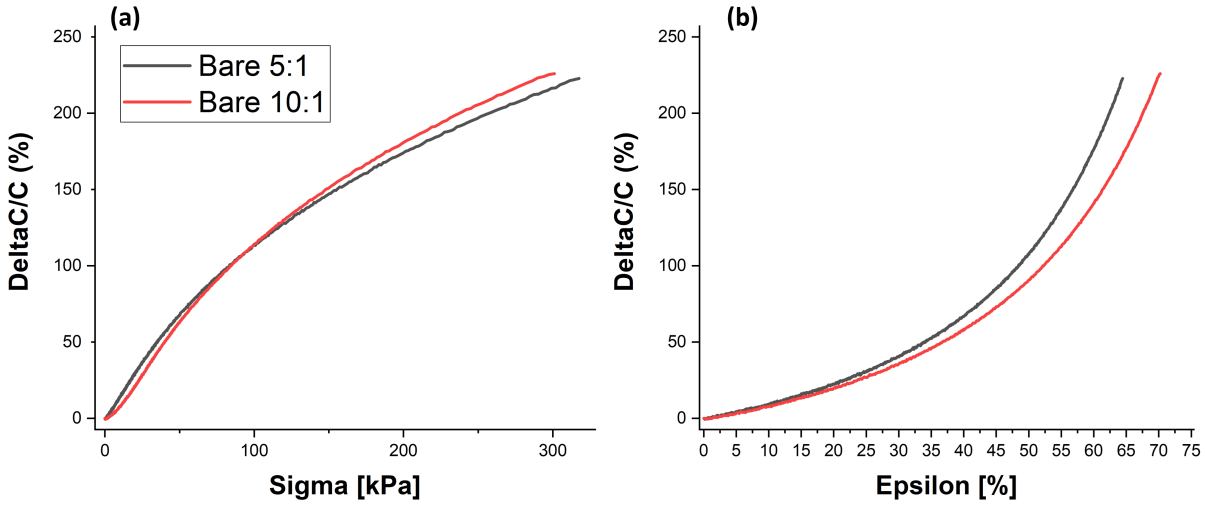

Figure 27 Bare 5:1 and 10:1 sponges comparison: relative change in capacitance versus (a)pressure and (b)relative percentage deformation

In the cyclic tests both samples proofed great electrical stability over time (fig28a) and a negligible hystheresis (fig28b-c).

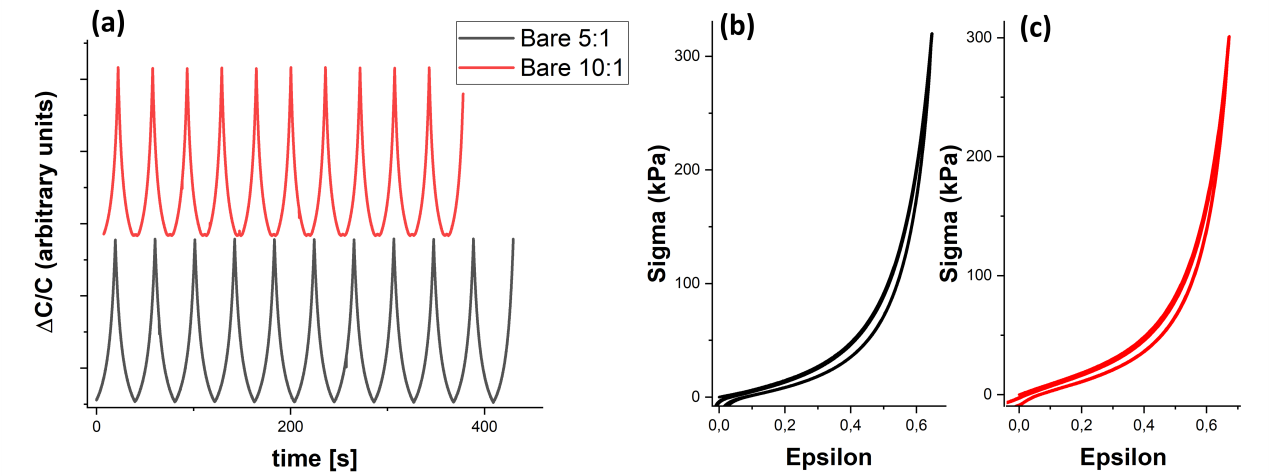

Figure 28 10 compression cycles of the bare 5:1 (black) and 10:1 (red) sponges: (a)time change of the relative variation in capacitance, (b-c)stress-strain curves

Having found that the samples have basically the same behavior, for all subsequent sponges the base elastomer to curing agent ratio was fixed equal to 5:1. Indeed, in the pre-curing phase an higher concentration of crosslinker makes the uncured PDMS less viscous and, as a consequence, easier to be adsorbed by capillarity in the sponge, also after the addition of conductive fillers that increase the degree of viscosity.

6.2 Metal precursor solution

As disclosed in the Decoration section, the metal precursor solutions were used to functionalize the sponges both by direct immersion in the solution, and by mixing the last with the uncured PDMS. In the first case, just the 5:1 sponge decorated by the solution of $AgNO_3$ 40 mM was packaged and analysed since lower $AgNO_3$ concentrations produced too few metal NPs. In the other case, 5 g of uncured PDMS were mixed with a $AgNO_3$ solution in a concentration of 10 mM, 20 mM, 30 mM and 40 mM. In figure 29a it can be observed a clear improvement in sensing performance passing from a 10 mM solution to a 30 mM one. The 40 mM solution sponges have proven to be surprisingly worse than the 30 mM, maybe because the reduction of metal precursors into NPs by the curing agent encountered a saturation. The 20 mM and 30 mM sponges explored the wider strain range (fig29b).

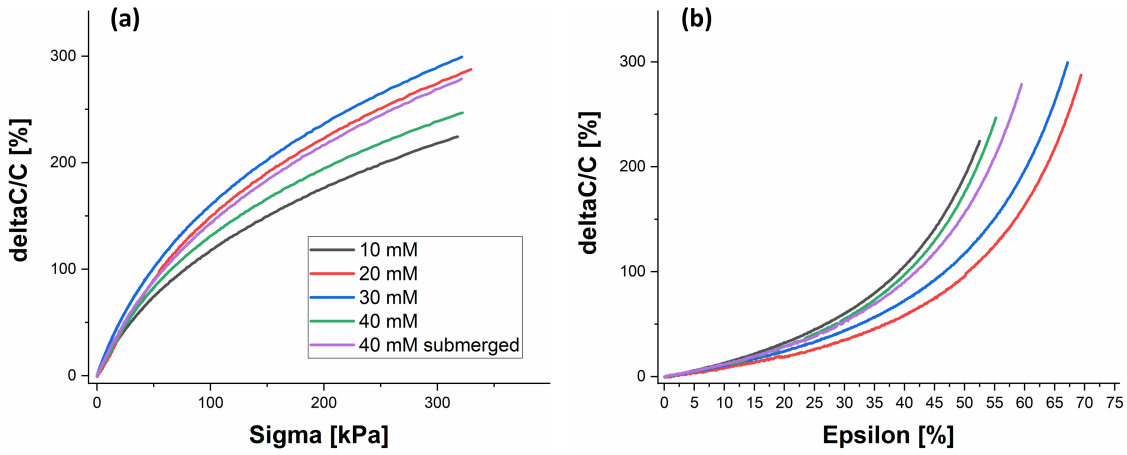

Figure 29 Relative change in capacity against (a)sigma and (b)epsilon of the samples functionalized with $AgNO_3$ solution $\{10, 20, 30, 40\}$ mM and the one submerged in a similar solution 40 mM

All the samples demonstrated a good stability in cyclic tests (fig30a) together with a negligible hystheresis (figure30b, c, d, e, f).

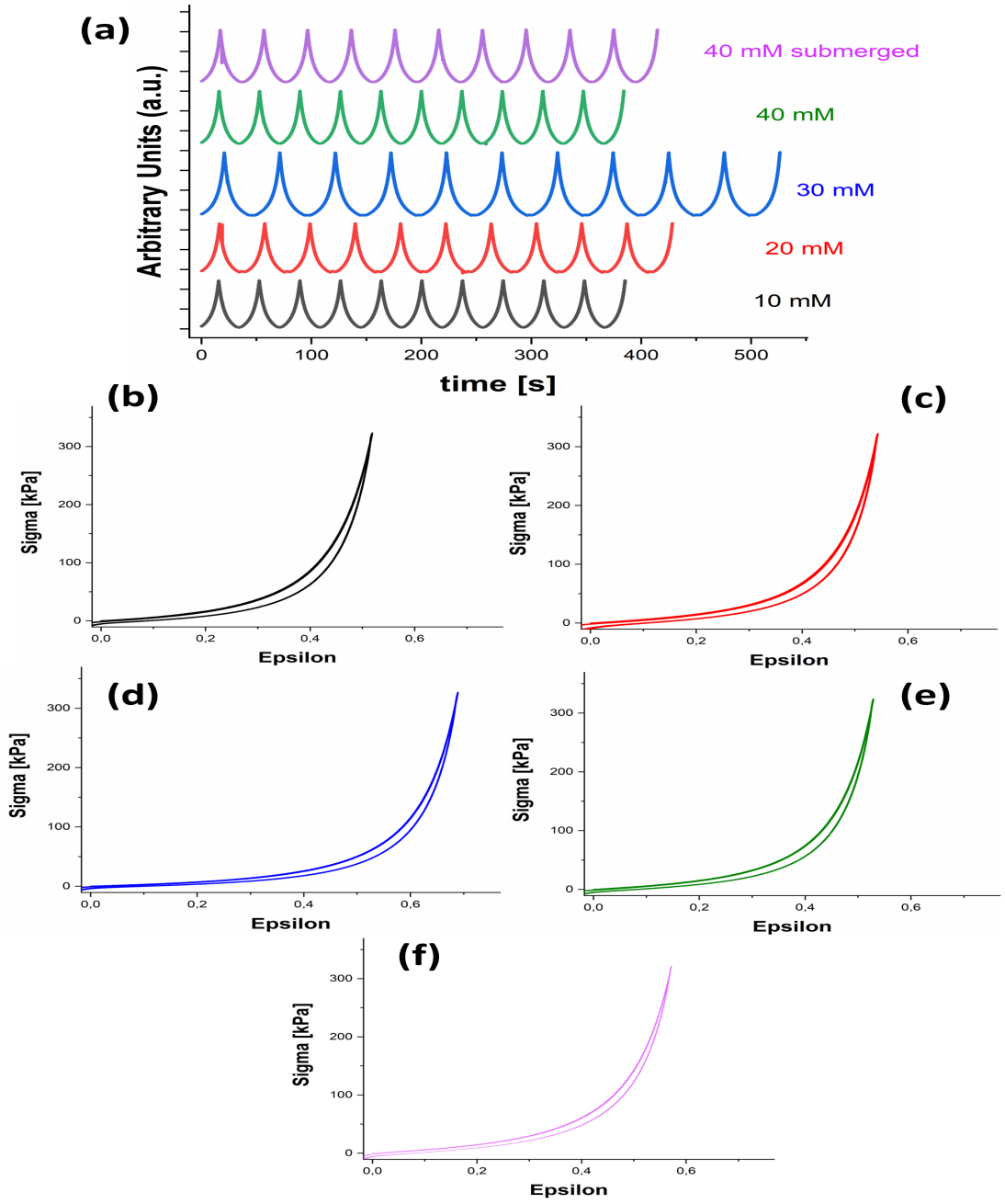

Figure 30 Relative change in capacity against sigma (a) and epsilon (b) of the samples functionalized with $AgNO_3$ solution $\{10, 20, 30, 40\}$ mM and the one submerged in a similar solution 40 mM

6.3 Conductive powders

With the aim of studying the impact over the sensing performances of the devices, three kind of conductive powders (silver nanoflakes, silver nanoparticles and carbon mesoporous microparticles) were added to the uncured PDMS as explained in the Addition of conductive nanofillers section, at several concentrations with respect to the uncured PDMS (whose quantity was set equal to 5 grams

for all subsequent preparations). The corresponding sponges will henceforth be referred to as X-Ywt%, where X is the acronym of the used powder (Ag nFls for silver nanoflakes, Ag NPs for silver nanoparticles and C meso-P for carbon mesoporous particles), and Y is the percentage of added powder compared to the weight of the polymer.

6.3.1 Silver nanoflakes

The silver nanoflakes powder was purchased from Alfa Aesar Company ®(fig31a). It was blend with the polymer at concentrations equal to 5wt%, 10wt%, 20wt%, 40wt% and 60wt%. The grey colour of the resulting sponges reflects that of the powder used, and going from 5wt% to 80wt% it changes from slightly darker to darker (fig31b).

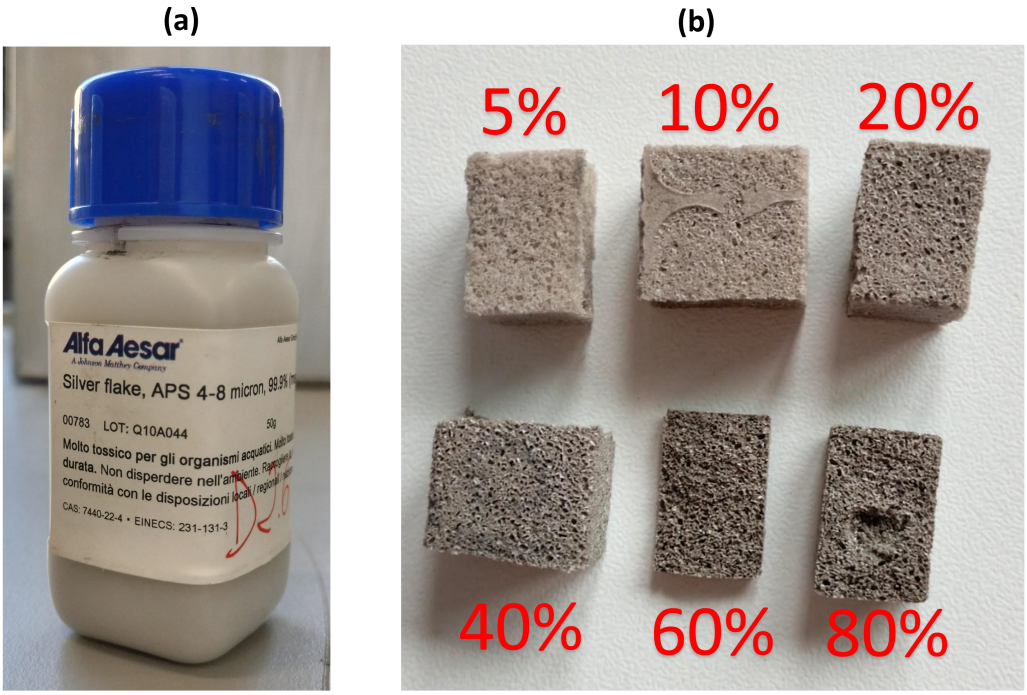

Figure 31 (a)Silver flake of the Alfa Aesar Company (b)Sponges with increasing concentration in weight of Ag nFl

Between the upper and lower curves in figure 32a there is a 100% increase in the relative change in capacity at the maximum pressure applied. This could be attributed to the fact that as the relative amount of powder added increases, the dielectric constant of the sponge increases and consequently also the sensitivity to pressure.

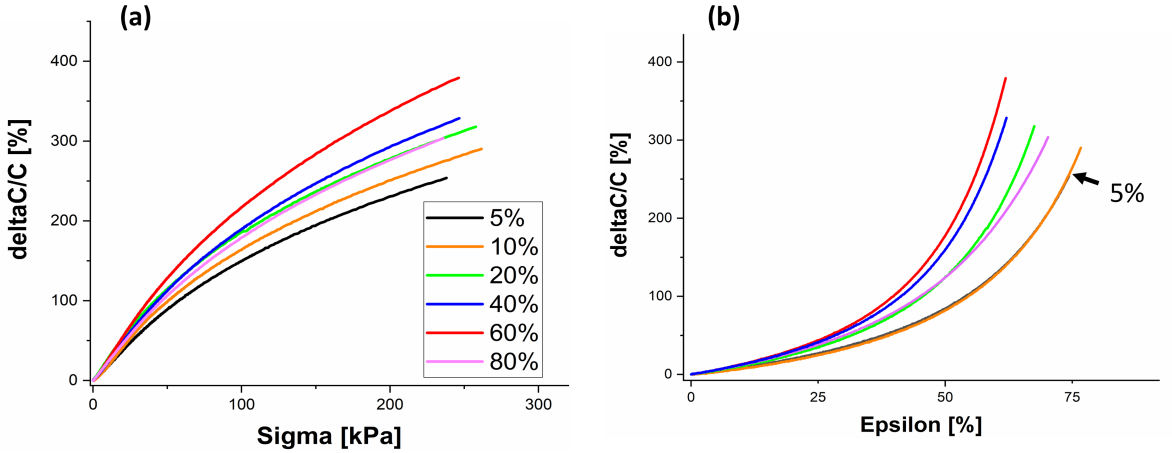

Figure 32 Relative change in capacity of silver nanoflakes functionalized device versus stress (a) and strain (b)

The 80% curve is comparable with the 20% one, and this could be related to a viscosity problem. The PDMS compound plus 80% powder is so viscous to be hardly adsorbed by capillary operation within the sponge, as evidenced in figure 33 where the holes correspond to zones just composed by sugar and consequently totally removed during the template dissolution step. Therefore, the actual concentration of nanoflakes embedded in the internal pores of the sponge is probably much less than 80%.

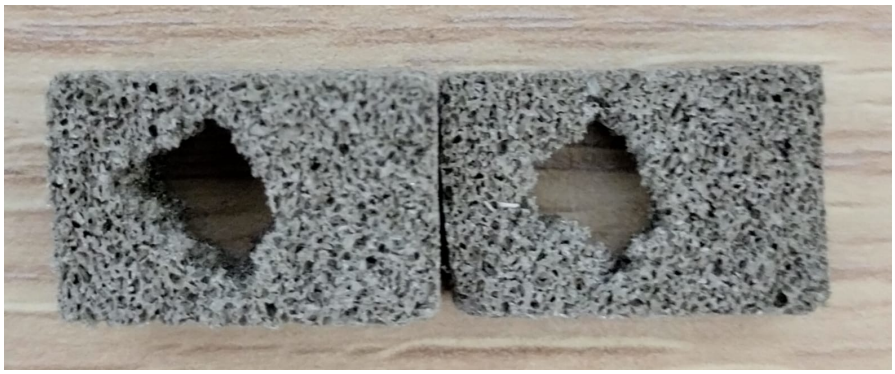

Figure 33 (80% sponge with holes inside due to partial infiltration of the PDMS plus powder compound

The incorporation of fillers in the sponge certainly modifies the mechanical properties. The greater the amount of fillers, the lower the elasticity. In figure 32b the strain percentage reduces from right to left, from the 5% to the 60% sample, except for the 80% special case. The cyclic tests did not deteriorate the performance of the devices as evidenced in figure 34a, moreover the hysteresis is negligible (fig34b, c, d).

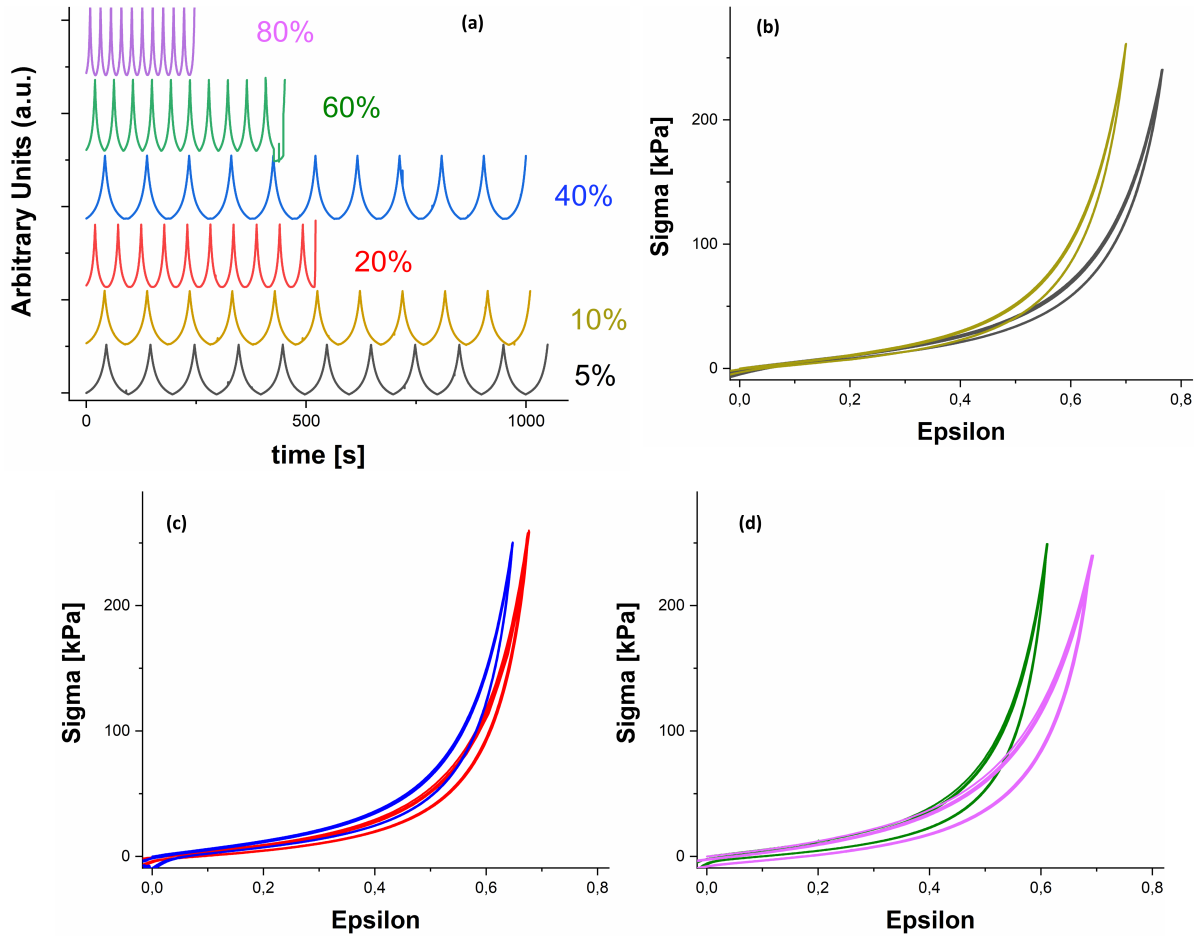

Figure 34 Cyclic tests of silver nanoflakes samples: (a)relative capacity change over time, (b, c, d) stress-strain curves

6.3.2 Silver nanoparticles

The silver nanoparticles were purchased from Taxco s.r.l. (fig35a) and a unique concentration of 40% in weight was tried because, in the case of nanoflakes, it ensured good sensing performance together with excellent miscibility between powder and uncured PDMS. The 40% Ag NPs sponge is shown in figure 35b. With respect to Ag nFl 40% sponge, the Ag NPs revealed slightly worse relative change in capacity (fig36a) and equal deformability (fig36b), together with good stability and small hysteresis (fig37).

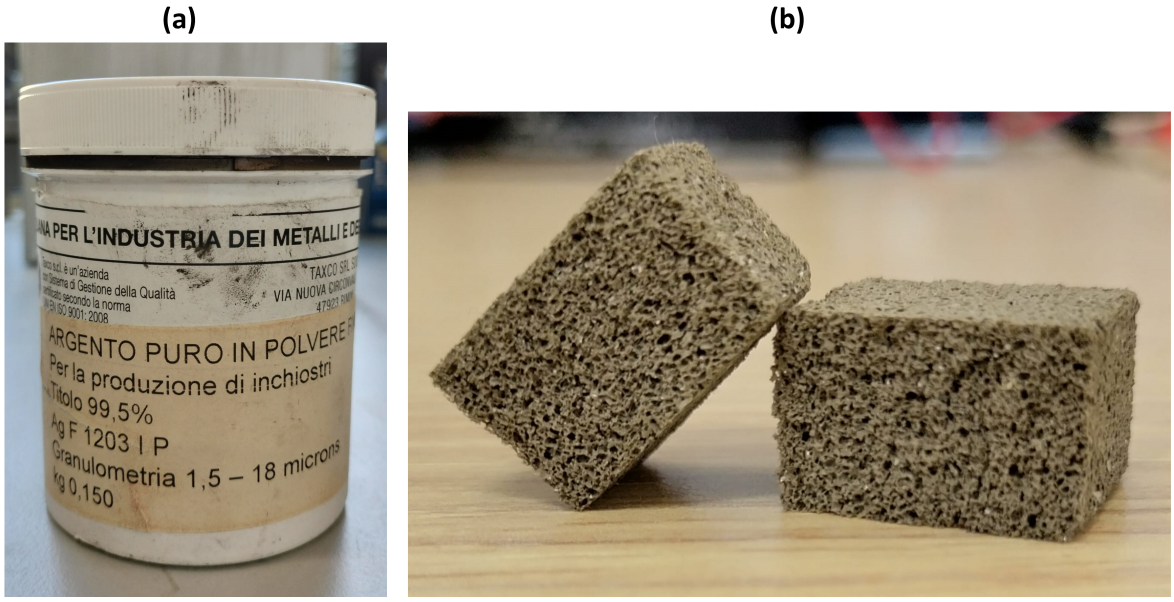

Figure 35 (a)Ag NPs of the Taxco s.r.l. and (b)relative sponge

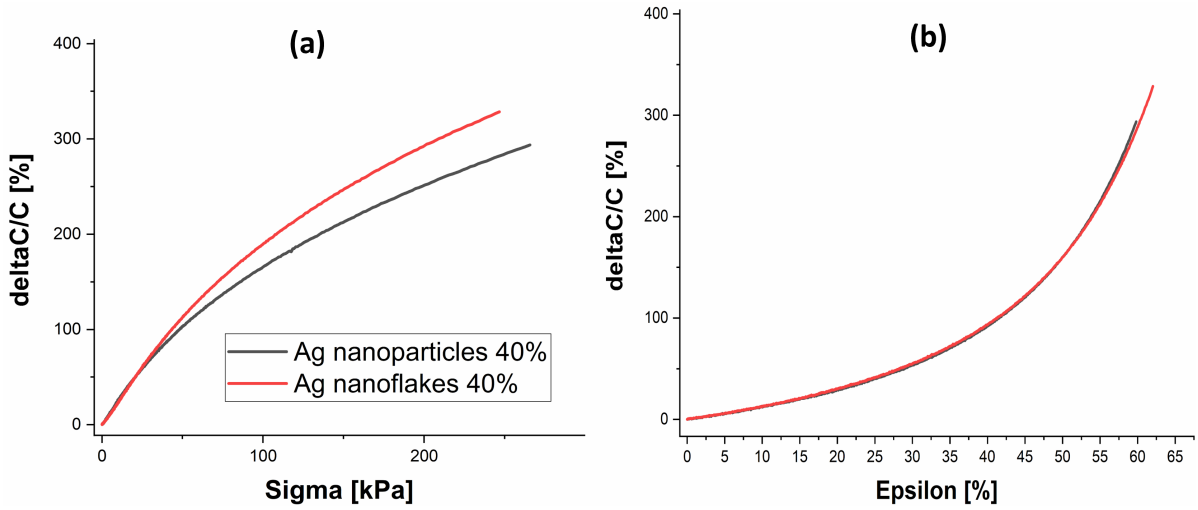

Figure 36 Samples with Ag NPs (black) and Ag nFls (red) at 40% of the polymer weight: relative change in capacity with respect to stress (a) and strain (b)

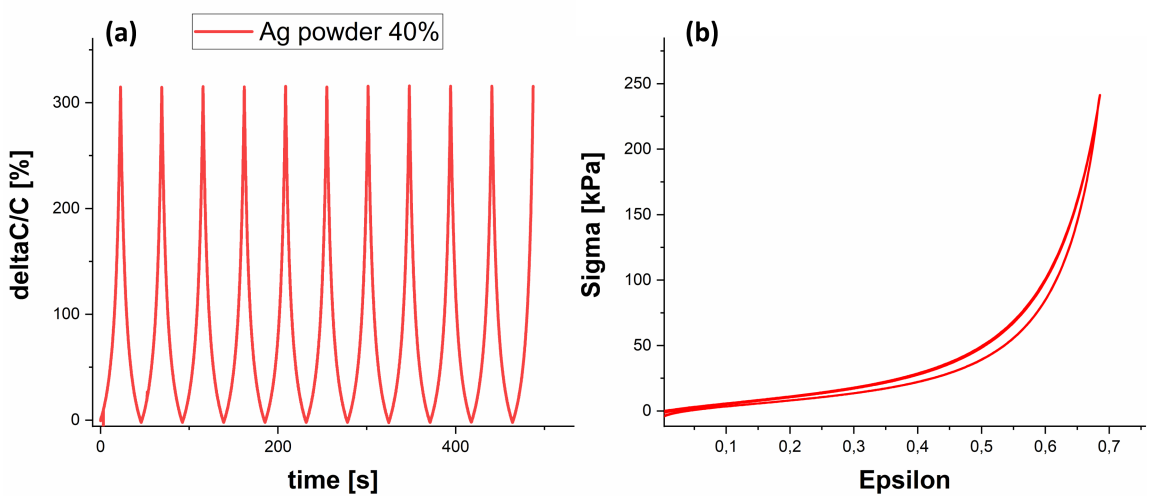

Figure 37 Compression cycles of the sample with 40% of the polymer weight of Ag NPs: (a)relative change in capacity in time (b)stress-strain curve

6.3.3 Carbon mesoporous particles

The carbon mesoporous particle powder was purchased from Sigma Aldrich (fig38a) and, initially, a 20% in weight was mixed to the uncured PDMS. Carbon has a low molecular weight (tab tab:powder tab) and, moreover, the NPs have inner pore which make them lighter, so the amount of powder was so much that the PDMS mix was too dense to be absorbed by the sugar cube. Indeed, the resulting sample was just an hollow shell of the original lump of sugar (fig38b).

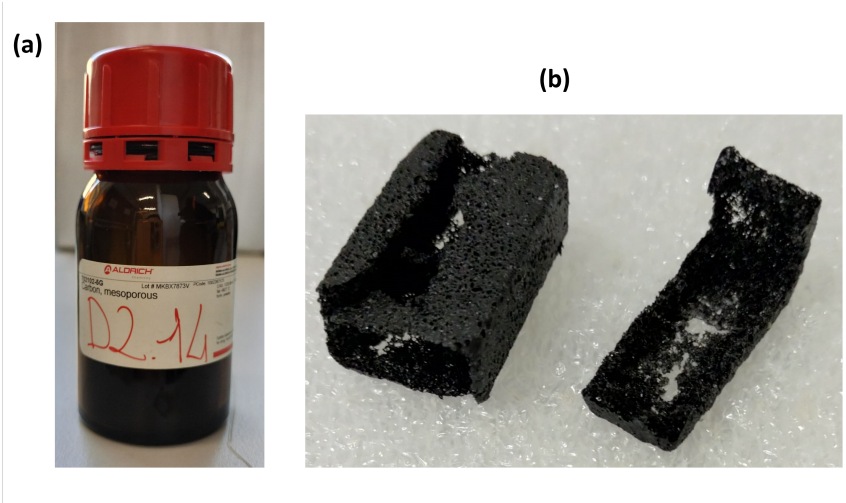

Figure 38 (a)Carbon mesoporous particle powder of the Sigma Aldrich and (b)20% carbon sponge

The maximum percentage concentration suitable to form a sponge was found to be 5% (fig39).

Figure 39 pPDMS sponge with 5% in weight of mesoporous carbon particles

The 5% carbon sample has similar electrical properties with respect to 30 mM $AgNO_3$ sponge (fig40), and it has mechanical stability and negligible hysteresis (fig41).

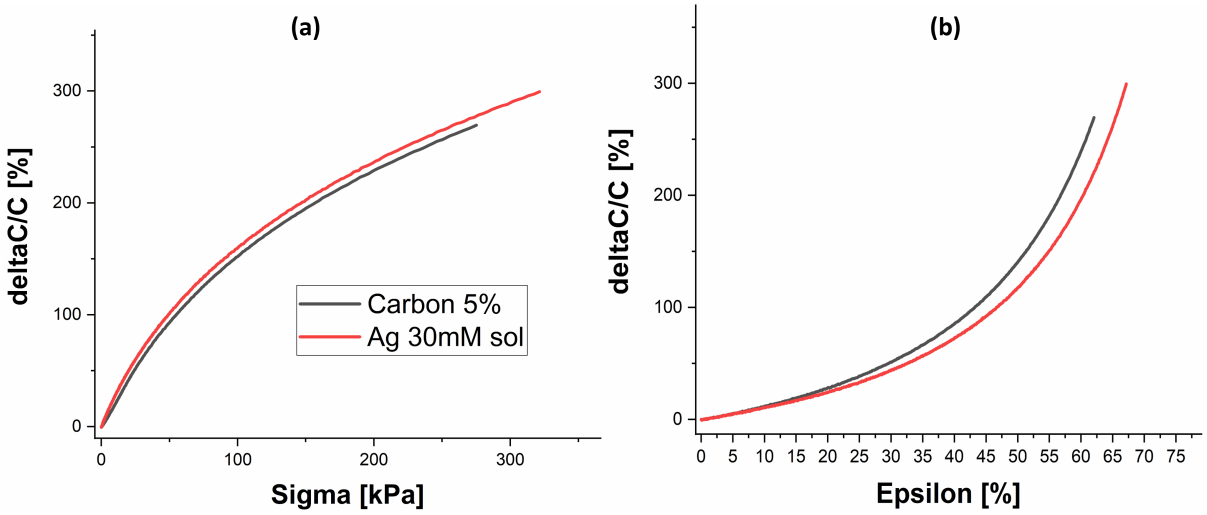

Figure 40 Samples with C mesoporous particles (black) at 5% of the polymer weight and $AgNO_3$ 30mM solution (red): relative change in capacity with respect to stress (a) and strain (b)

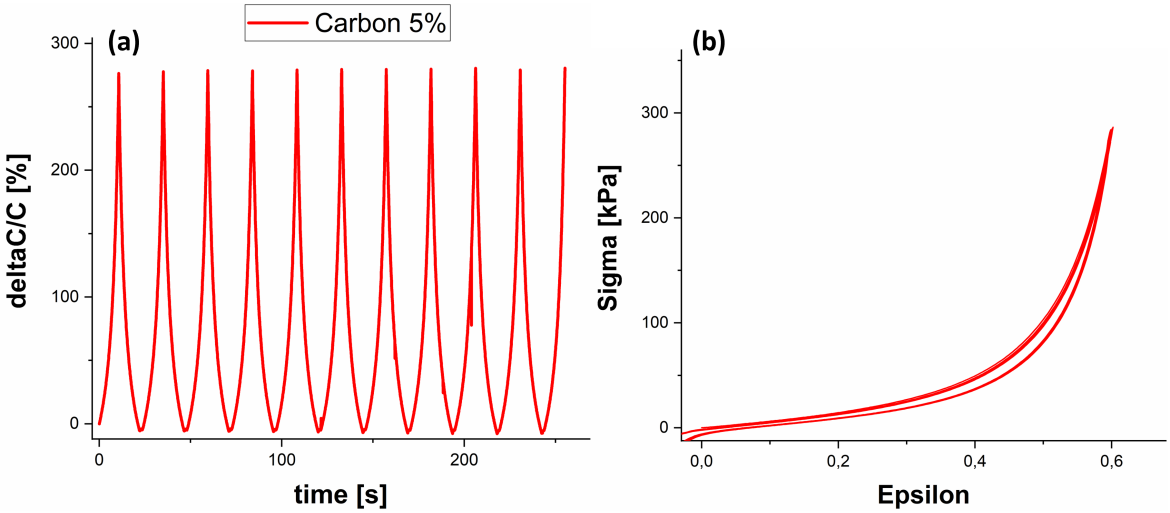

Figure 41 Compression cycles of the sample with C mesoporous particles at 5% of the polymer weight: (a)relative change in capacity in time (b)stress-strain curve

6.4 Template comparison

In this section a comparison among the best templated samples is presented. Of all the conductive fillers, the most effective were found to be the silver nanoflakes, particularly in concentrations of 40% and 60% by weight, since they provide the greatest relative change in capacity, at the same pressure (fig42). In terms of limit of detection (fig43a) almost all the conductive fillers gave excellent outcomes, with the lowest weight sensed around (Ag nFl 40% and 60%) or even under 1 gram (C 5%, bare 5:1 and Ag NP 40%).

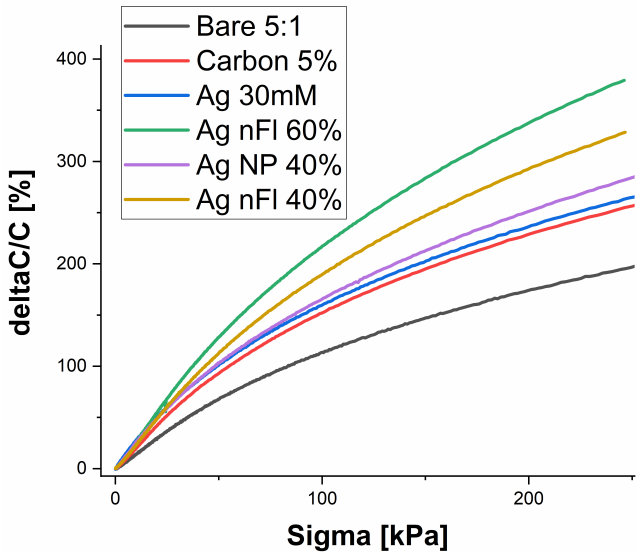

Figure 42 Comparison among the best template samples: relative change in capacity with respect to stress

The sensitivity is related to the slope of the $\Delta C/C$-σ curve, and changes according to the interval

of pressures considered. The bar graph 43b reports the sensitivity in three consecutive pressure ranges. The progressive flattening of the plots in figure 42 justifies the global reduction of sensitivity with increasing pressure range. Furthermore, no sample greatly prevails over the others, meaning that the $\Delta C/C$-σ curves are almost all parallel to each other, considering a limited section of plot. As far as Young's Modulus is concerned, it is convenient to open a wider parenthesis. Contrary to expectations, the bar graph in figure 43c shows that the stiffest sponge, i.e. with the largest Young's Modulus, turns out to be the bare 5:1, devoid of any filler. Instead, it would be more reasonable for sponges with solid and therefore rigid nanofillers to be less soft. The discourse changes by looking at Young's Modulus at the end of the stress-strain curve (red box in the inset of figure 43d). The softest sponge is now the bare 5:1 while the others all have more or less the same Young's Modulus. The difference could be attributed to the variation in the sponge's behavior depending on the compression regime. In the first part of the stress-strain curve (inset in figure 43c), the compression of the sponge involves the progressive expulsion of the air contained in the pores until it is exhausted, with the consequent closure of all pores. A reasonable explanation behind the graph in figure 43a could be that the higher degree of viscosity achieved by the PDMS with the addition of nanofillers hindered the infiltration into the sugar cube to such an extent that it was incomplete at a microscopic level. At this point, areas were created inside the cube without PDMS, which were completely removed by washing in water. These empty areas helped to make the sponges with nanofillers even more porous, and therefore mechanically weaker and softer, compared to the bare 5:1 where the less dense PDMS penetrated more effectively. This is why the sample has a greater "porous" Modulus of Young. After closing all the pores, the sponges behaved as a solid block of PDMS. The compression of the "bulk" sponge (i.e. the "bulk" Young's Modulus) only highlighted the differences between the PDMS constituting the sponges, so that the samples with nanofillers were reasonably stiffer. However, the real motivation may be more subtle and would require further investigation.

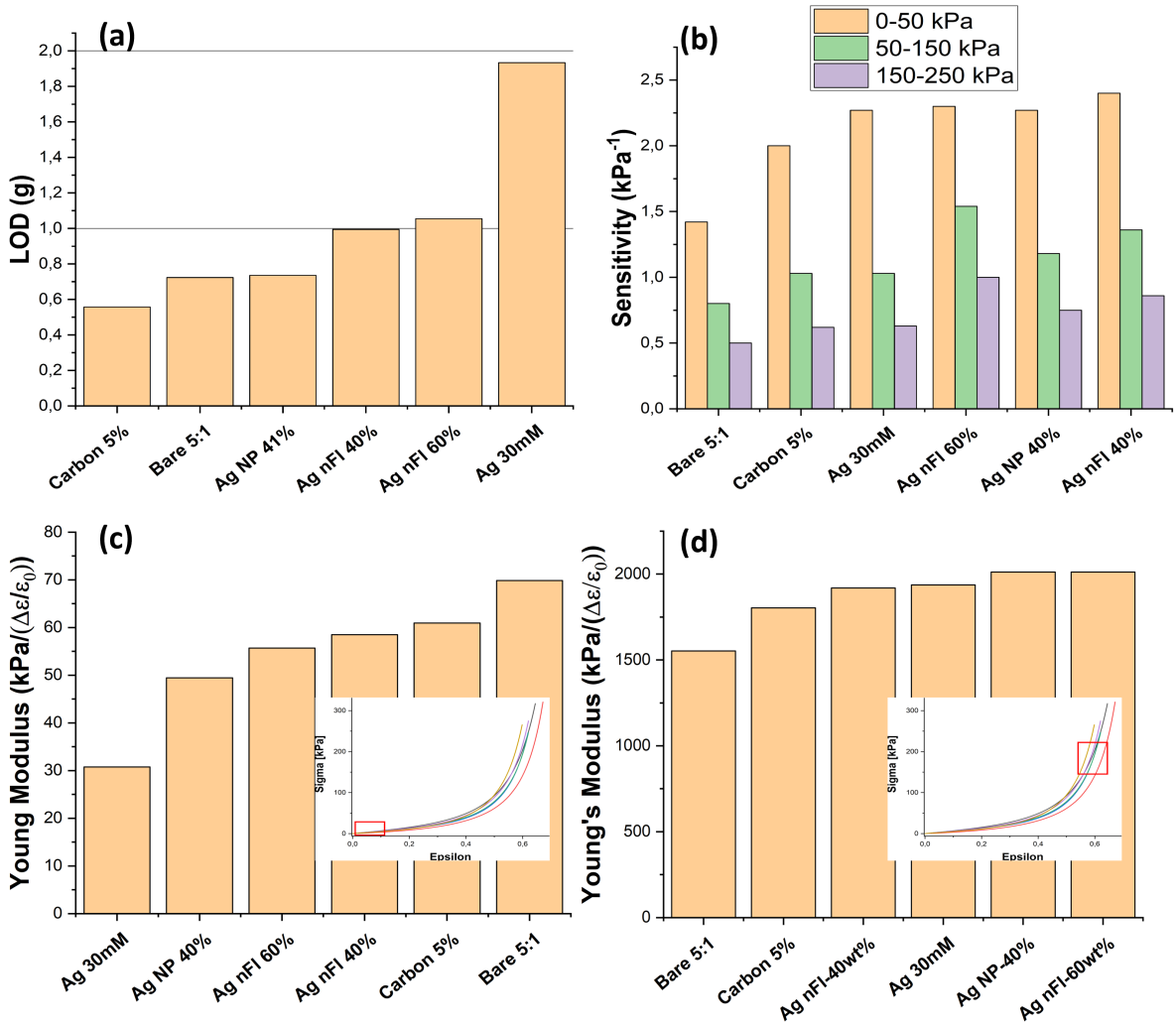

Figure 43 (a)Limit Of Detection (b)sensitivity at several pressure ranges (c)"porous" Young's Modulus (d)"bulk" Young's Modulus

Some samples were also studied at rest with the Scanning Electron Microscope (SEM) to observe on a micrometric scale the internal porous structure and the various fillers used. All the sponges were found to share the same architecture of the bare 5:1, at a micrometric scale: an open-cell structure (fig44a) with large pores several hundreds of microns wide (fig44b).

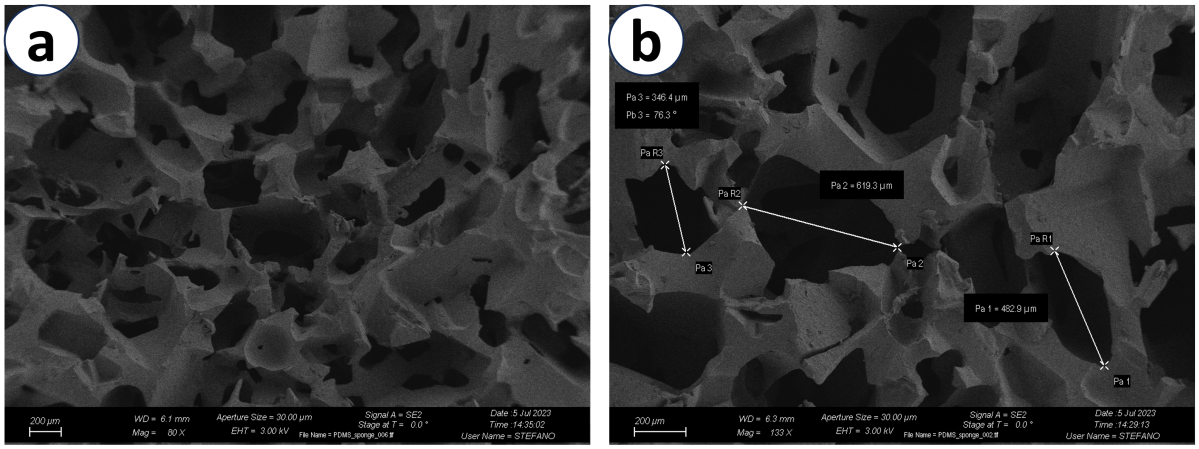

Figure 44 SEM image of the inner porous structure of the bare 5:1 sponge(a) and a further magnification(b)

As can be observed in figure 45a and in the zoom on the right (fig45b) the silver nitrate 30 mM sponge had rounder and softer pore edges with respect to the bare one. This could be attributed to the residual water of the solution mixed with the uncured PDMS, and later incorporated within the lump of sugar by capillarity, causing a partial dissolution of the inner sugar crystals.

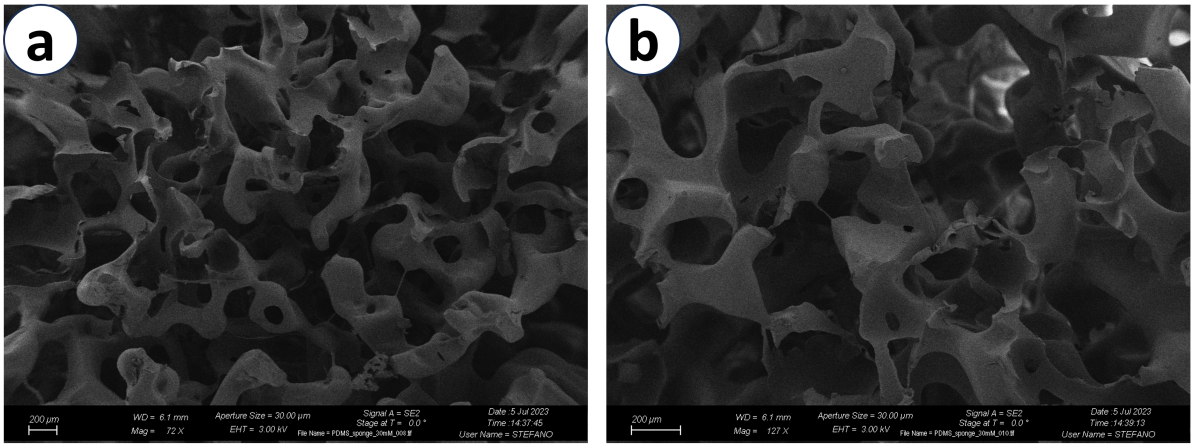

Figure 45 SEM image of the inner porous structure of the $AgNO_3$ 30 mM sponge(a) and a further magnification(b)

The reduction of silver nitrate by the PDMS cross-linking agent with the consequent incorporation of agglomerates of silver particles on the pores of the sponge is highlighted in images 46a-c together with the corresponding zooms 46b-d. The agglomerates size is highly variable, from a few to tens of microns.

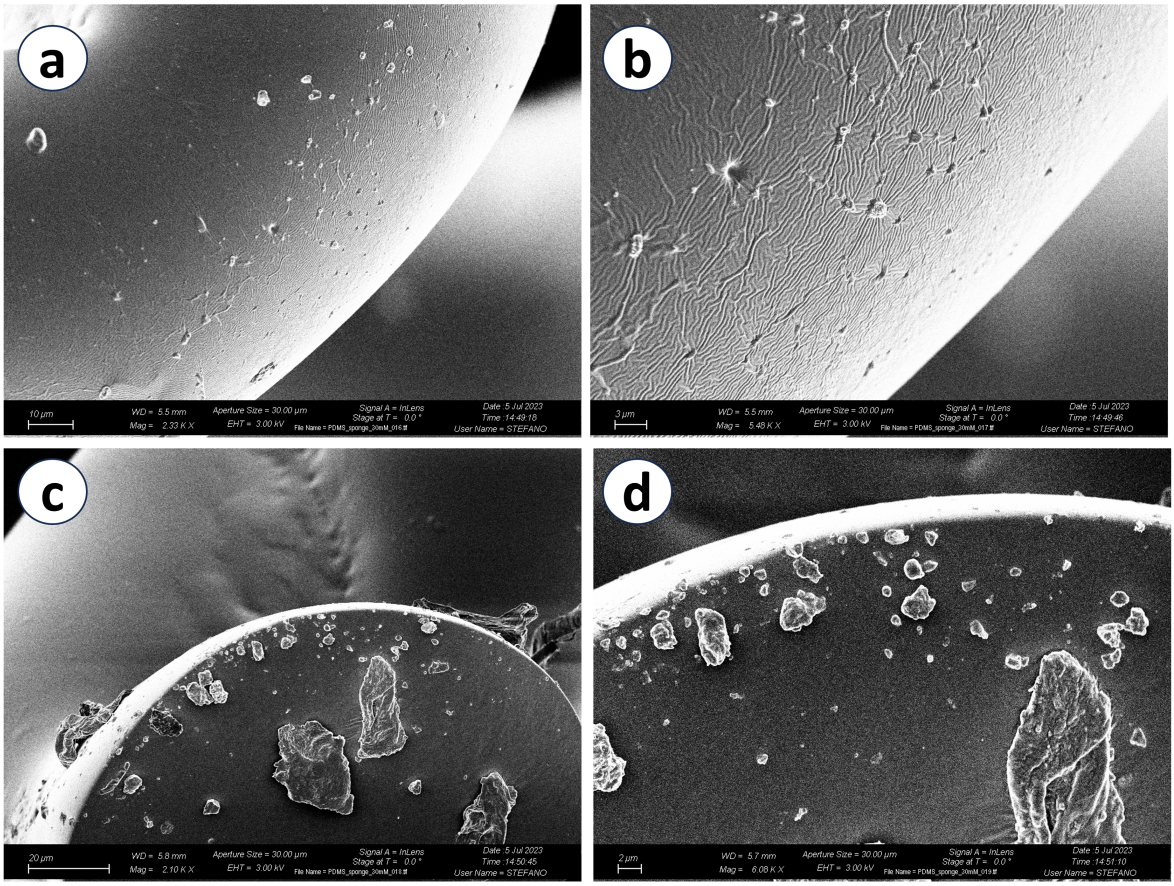

Figure 46 $AgNO_3$ 30 mM sponge SEM images of the agglomerates silver particles (a, c) and relative zoom (b, d)

The SEM inspections of the Ag nFl 20% (fig47a), 40% (fig47b) and 60% (fig47c) samples revealed an internal pore size and distribution almost indistinguishable from the bare one in figure 44a.

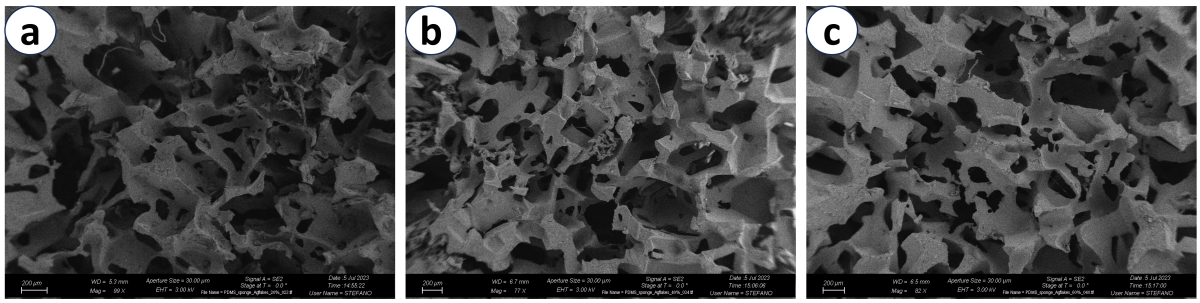

Figure 47 SEM images of Ag nFl sponge at a concentration equal to 20%(a), 40%(b) and 60%(c)

The image 48a clearly proofs the presence of the silver nanoflakes with an almost two-dimensional and irregular shape quite distinct from the probable impurities that look more like specks of dust. Image 48b offers a further magnification on a few flakes.

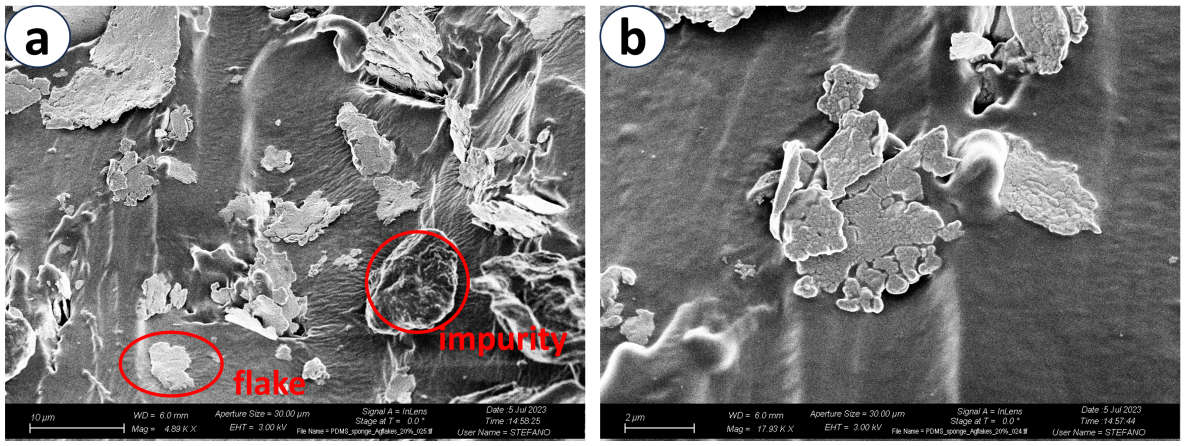

Figure 48 Caption

The increase in the concentration of silver flakes is clearly visible in the random acquisitions of the pore surfaces of sponges at 20%, 40% and 60% respectively in figures 49a, 49b and 49c. The flakes are not only adhered to the outer surface of the pores, but also inside the PDMS as shown by the zoom (fig49d, red circles) on the sloping flakes because they are partially inside the polymer.

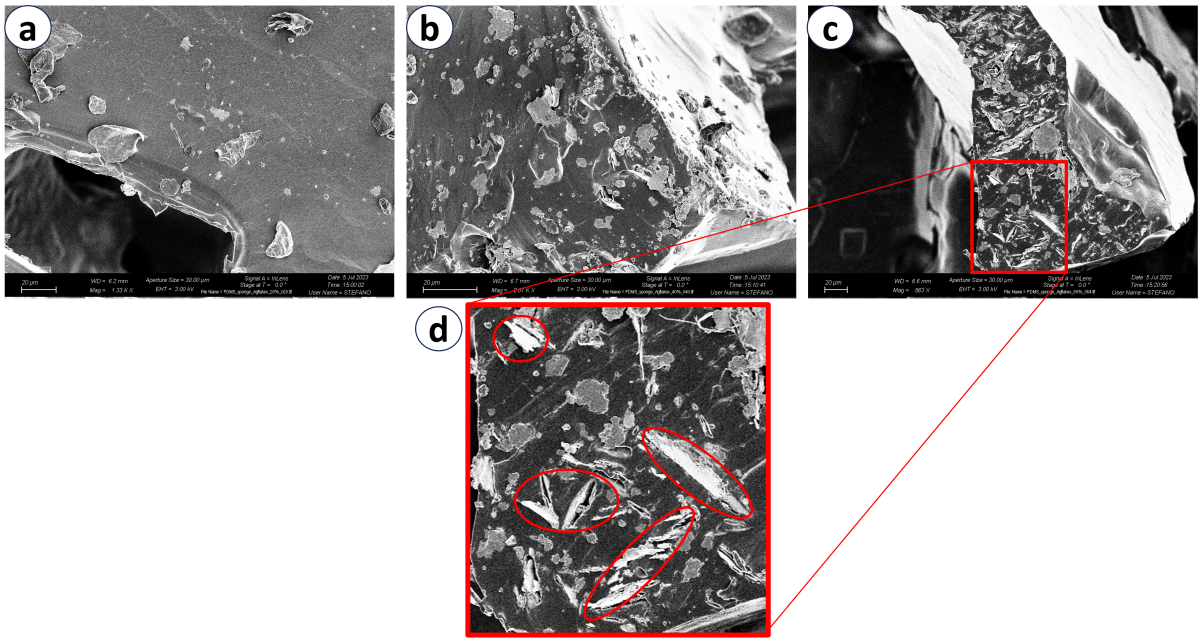

Figure 49 SEM images: pores surface of the Ag nFl 20%(a), 40%(b) and 60%(c) samples; (d)zooming in on piercing flakes (red circles)

The Ag NP and C samples are characterized by the usual large open-cell micro structure (fig50a-d, respectively). Both the Ag NPs (fig50b, red circles) and the C particles (fig50e) have irregular shapes and are distinguishable from the background and the impurities by the lighter color, a symptom of a different emission of electrons, collected by the SEM. The detail of a single C particle is

shown in figure 50f. Some Ag NPs look more like flakes (fig50c red circles). Finally, the qualitative concentration of Ag NPs seems comparable to those of the Ag nFl 40% sample in fig47b, and unsurprisingly so are their performances (fig fig:all c sigma epsa).

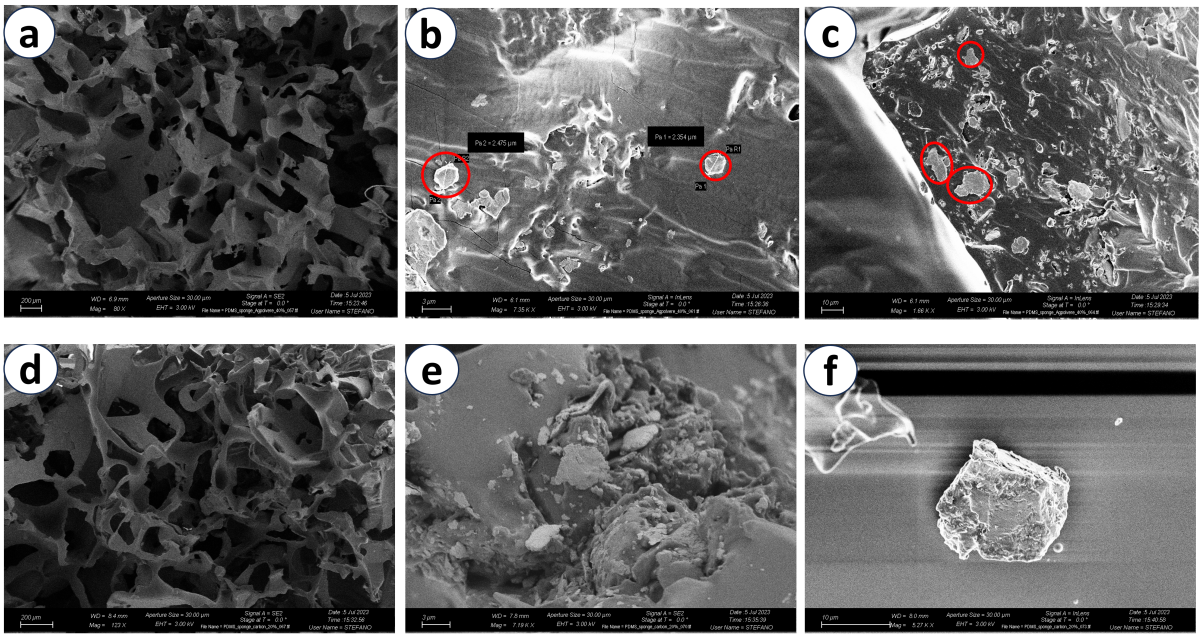

Figure 50 Caption

7 Results: mold sensors

Herein, a further distinction according to the used sugar molding method, as explained in the Materials and Method chapter, is made.

7.1 PDMS and sugar mix

Commercial soft white sugar was mixed with uncured PDMS in a 3:1 and 4:1 ratio to form foams from now called respectively 3:1 and 4:1 sponges. First of all, the bare mold sponges without any conductive filler inside are analyzed.

7.1.1 Bare mold sponges

The bare PDMS-sugar mix was poured into cases of the shape of a dog bone and rhomboid, respectively in figures 51a and b.

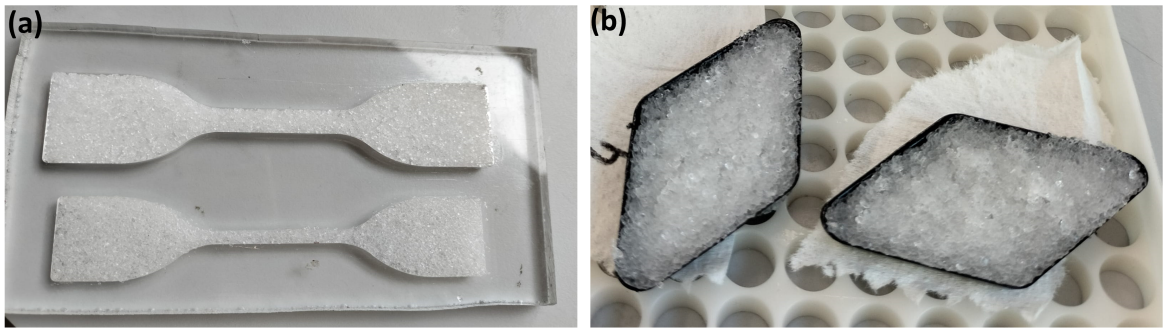

Figure 51 Molds: (a)dog bones, (b)triangles

The resulting sponges inherited the mold shape as highlighted in figure 52a, where some parts of the samples were already cut to assemble the pressure sensors. To demonstrate the spongy behavior, the samples were subjected to compression and torsion, respectively in figures 52b and c.

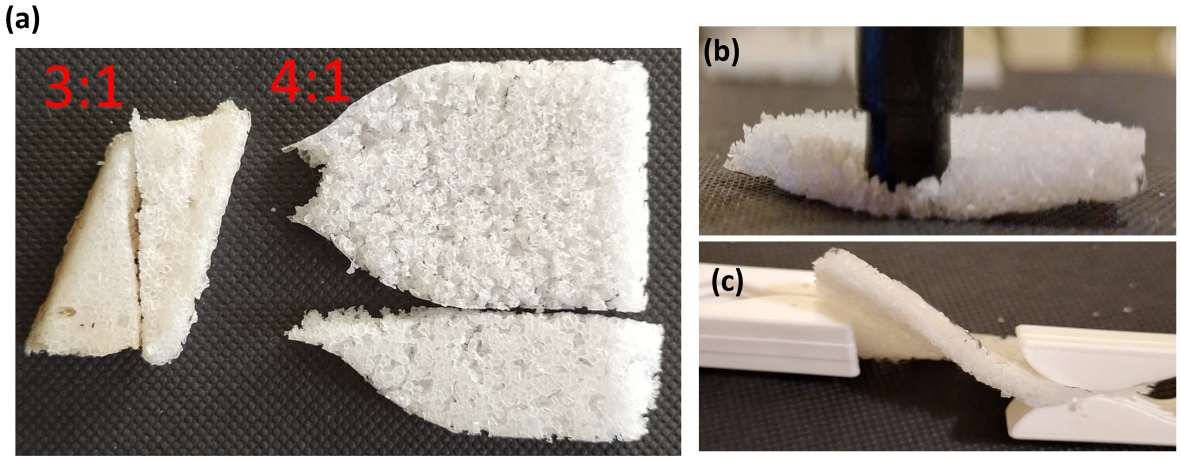

Figure 52 (a)Bare 3:1 (left) and 4:1 (right) sponges, (b)compression and (c)bending tests

The 4:1 sponge revealed to be the best stress (fig53a) and strain (fig53b) sensor, with respect to both the 3:1 mold sample and the bare template one (blue curve).

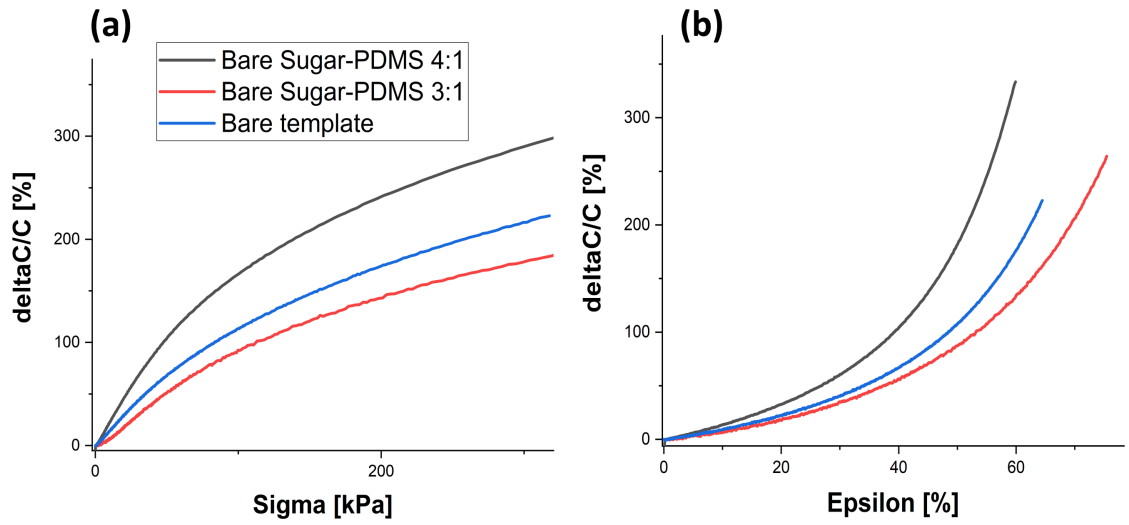

Figure 53 Relative change in capacity with respect to stress(a) and strain(b) of the samples: bare template (blue), 3:1 (red) and 4:1 (black) sponges

The casting process did not affected neither the electrical stability (fig54a) nor the hystheresis (fig54b-c).

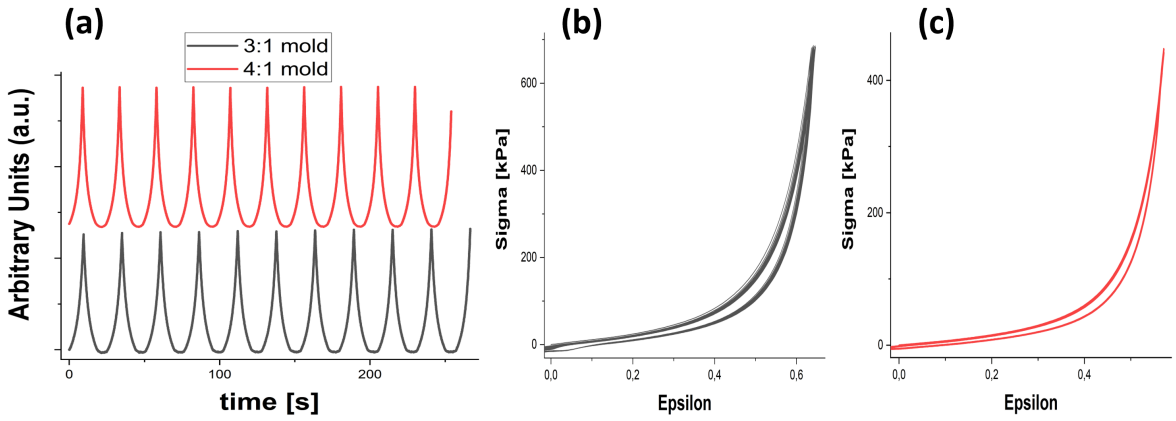

Figure 54 3:1 and 4:1 mold sponges cyclic tests: (a)$\Delta C/C$ versus time, (b) and (c)stress-strain curves

7.1.2 Ag nFls mold sponges

Successively the PDMS-sugar mixture was also added with Ag nFls since they proved to be the conductive filler providing the best sensing performances (fig fig:all c sigma eps a). Both the 3:1 and 4:1 sponges were modified with Ag nFls at a polymer weight ratio of 40% and 60%. The corresponding samples will henceforth be referred to as 3:1-Ag nFls-Ywt% and 4:1-Ag nFls-Ywt%, where Y is the percentage of added powder compared to the weight of the polymer. The cases were again dog bones and rhombuses (respectively in fig55a and b). The corresponding 3:1 sponges are shown in figure 55c, with on the left the Ag nFls-40wt% samples and on the right the 60wt% ones, which were partially cut to assemble the sensors.

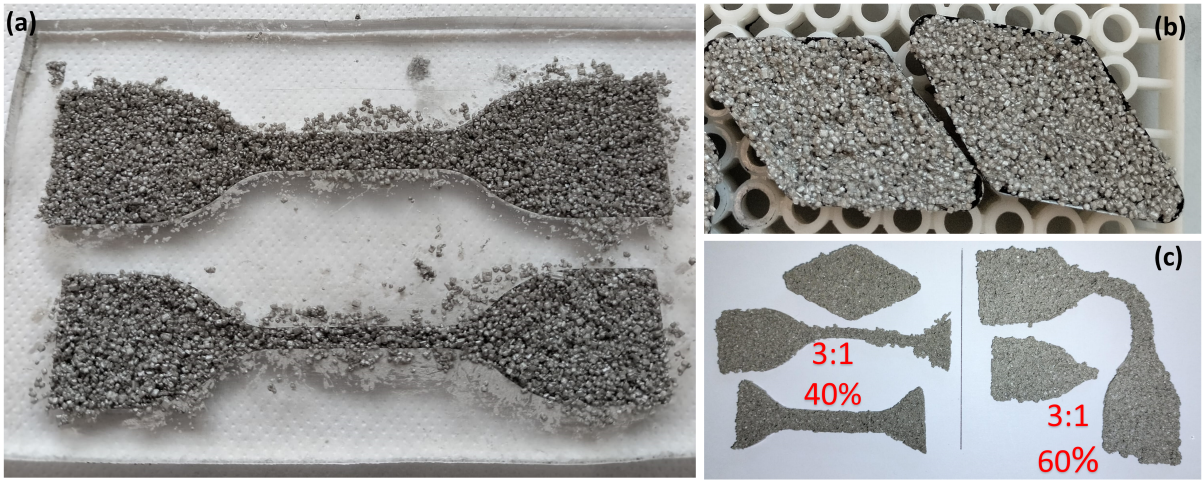

Figure 55 Mixture of uncured PDMS, sugar and Ag nFls in dog bones(a) and triangles(b) molds. (c)3:1 Ag nFls-40wt% (left) and 60wt% (right) mold sponges

The incorporation of Ag nFls at 40% by weight of the polymer in the Sugar-PDMS 4:1 mix was also successful (fig56a), while the concentration of 60wt% gave some problems. The first trial outcome was more like a very sticky membrane rather than a sponge, so much so that it was possible to shape it into a ball (fig56b). The second attempt at synthesis produced a non-continuous sponge, i.e. full of large holes (fig56c, d). So, just the 4:1 mold sponge with 40% Ag nFls was packaged as a pressure sensor.

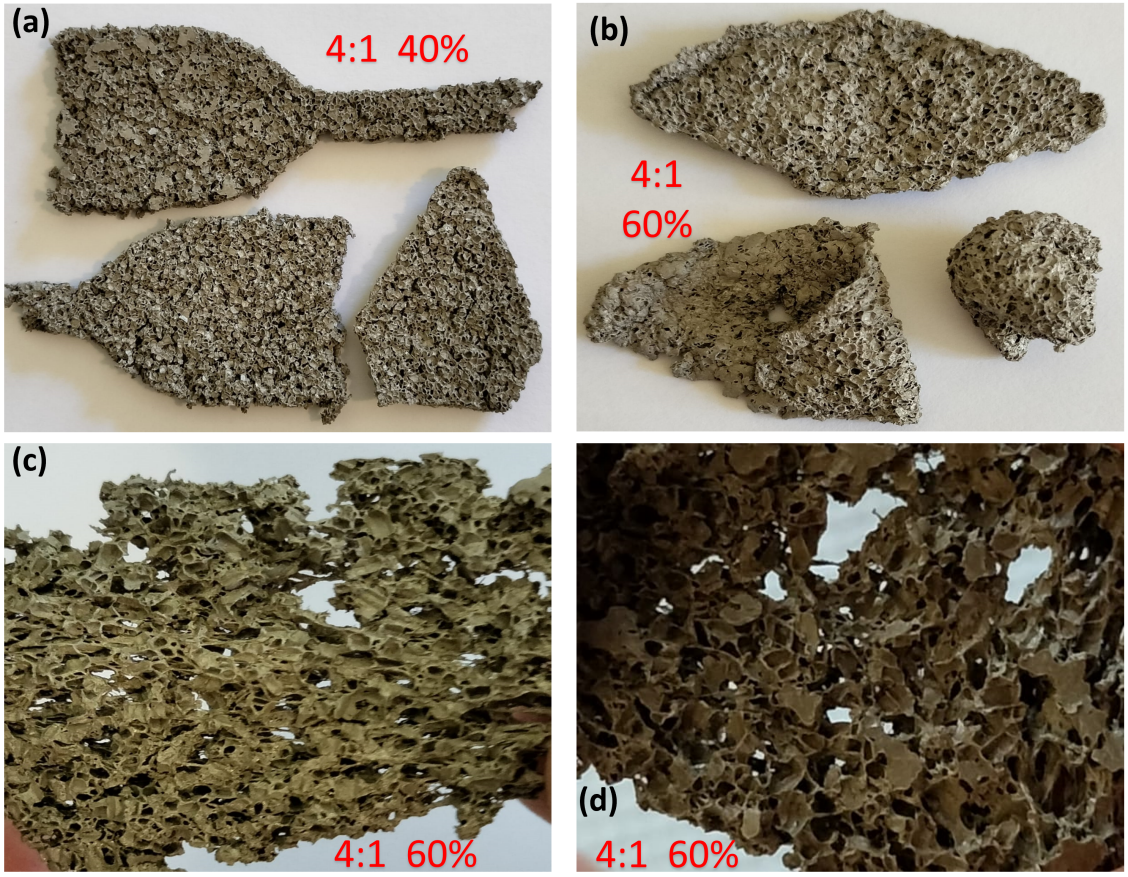

Figure 56 (a)4:1 mold sponge with 40% of Ag nFls (b)4:1 mold sponge with 60% of Ag nFls, first trial (c-d)4:1 mold sponge with 60% of Ag nFls, second trails

The 3:1-Ag nFls-40wt% and 4:1-Ag nFls-40wt% demonstrated comparable performances as stress (fig57a) and strain (fig57b) sensors. The 3:1-Ag nFls-60wt% sample showed slightly better pressure sensing performance, according to the higher amount of silver nanoflakes embedded within the porous polymer matrix (fig57a).

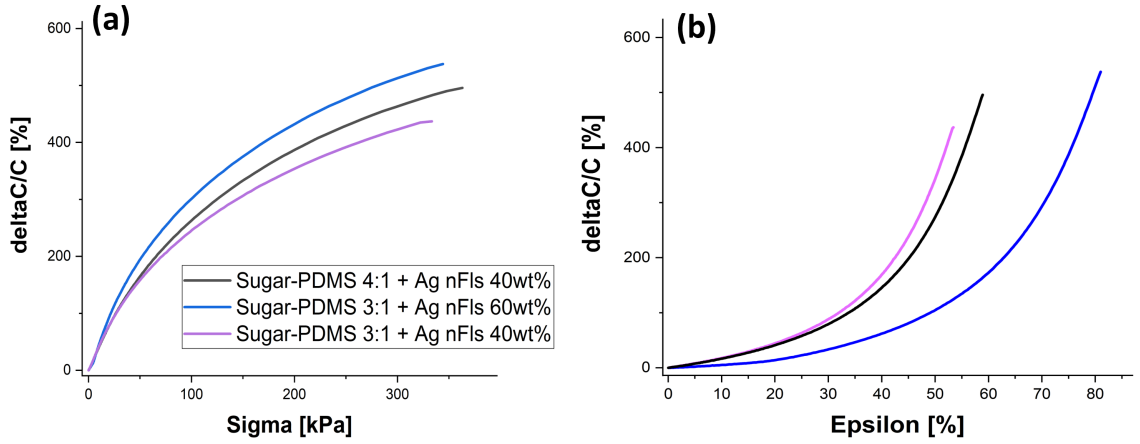

Figure 57 3:1 sponge with Ag nFls at 40wt% (purple) and 60wt% (blue), and 4:1 Ag nFls-40wt% (black) samples: relative change in capacity with respect to stress(a) and strain(b)

All the samples were characterized by a stable electrical signal during compression cycles (fig54a) and limited hysteresis (fig54b).

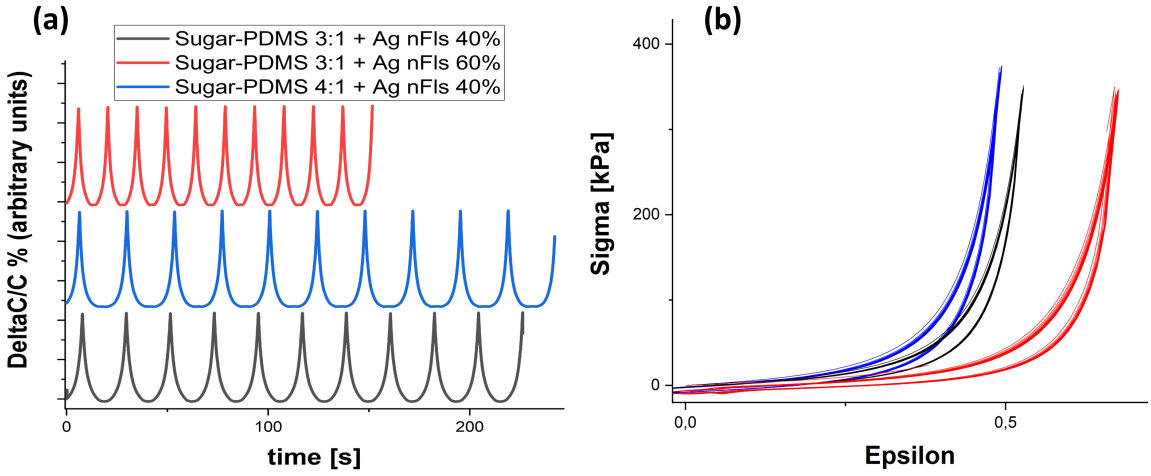

Figure 58 Compression cycles of the 3:1 sponge with Ag nFls at 40wt% (black) and 60wt% (red), and 4:1 Ag nFls-40wt% (blue) samples: (a)relative change in capacity over time and (b)stress-strain curve

7.2 Homemade sugar cube

The use of an homemade sugar cube was investigated as an alternative to a commercial standard one. A diamond mould was used to shape the sugar cube.
FOTO
Once formed, the casted lump of sugar was subjected to steps from 3 to 6 of the list above, and the base elastomer to curing agent ratio was fixed to 5:1. The single run tests highlighted that the homemade sugar cube and the commercial sugar cube sponges had almost coincident detection

performance in terms of pressure (fig59a), while the former was better in terms of strain sensitivity (fig59b).

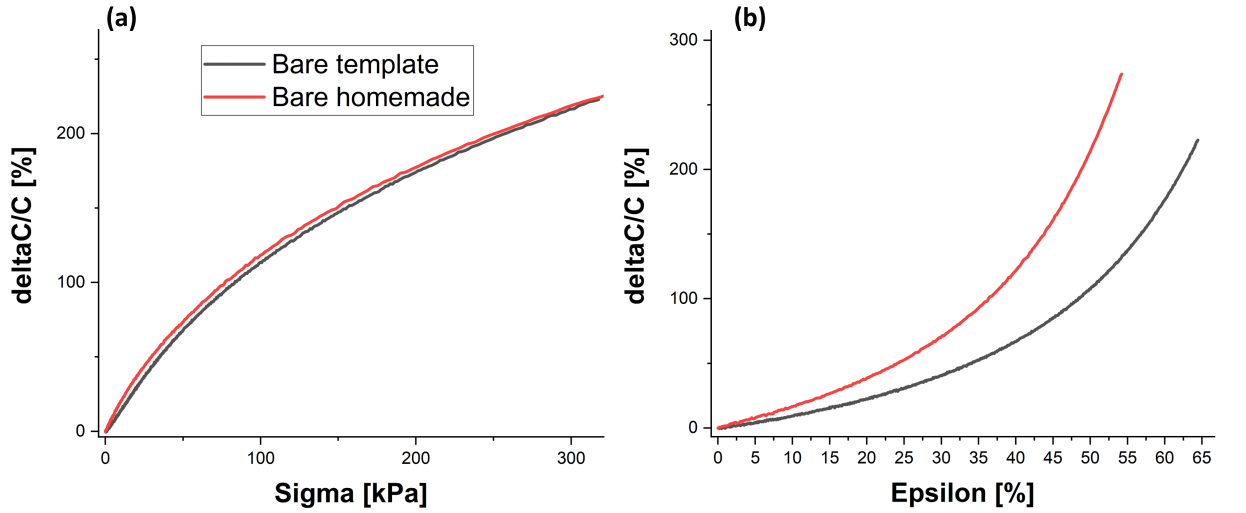

Figure 59 5:1 sponges realized with a commercial (black) and homemade (red) sugar cube, without any conductive filler: relative change in capacity versus (a)stress and (b)strain

Due to the strong affinity in terms of pressure sensitivity the homemade sugar cube sponge was not further modified with conductive fillers, to avoid replicating the already seen results. As usual, good electrical stability and small hysteresis characterized the sample (fig60a, b respectively).

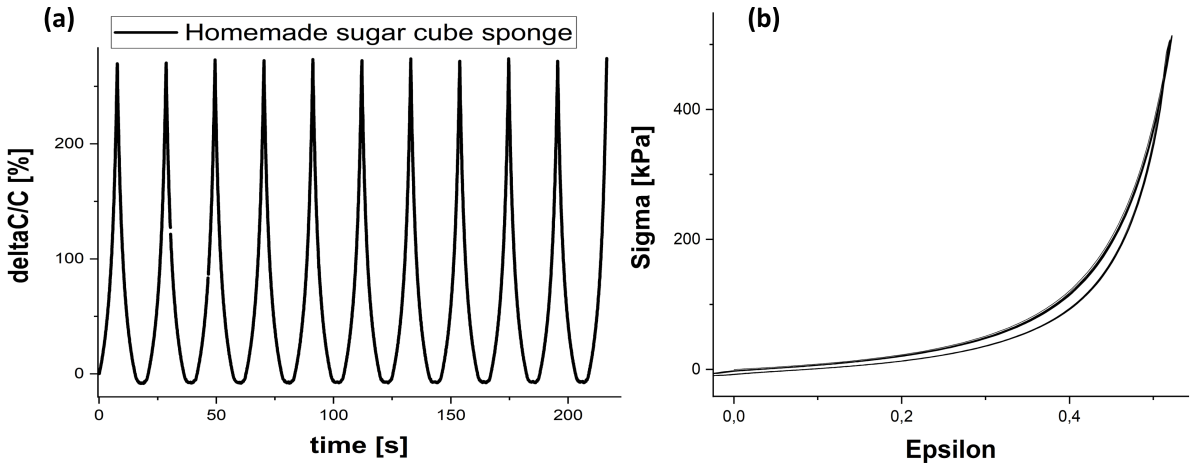

Figure 60 Compression cycles of the homemade sugar cube sponge without any conductive filler: (a)relative change in capacity over time and (b)stress-strain curve

7.3 Mold vs homemade comparison

Now, a comparison among the samples produced with a sugar molding approach is presented. As long as no conductive filler is added, the homemade sugar cube process provides a sponge with

comparable pressure sensing characteristics with respect to the PDMS and sugar mix one, as shown in figure 61a. The addition of silver nanoflakes, instead, totally change the situation (fig61b). Nevertheless, the homemade sugar cube sponge had the lowest LOD, lower than half gram (fig61c). The 3:1-Ag nFl-60wt% sample demonstrated to be the most sensitive device in each pressure range (0-50 kPa, 50-150 kPa and 150-250 kPa (fig61d). As for the Young's Modulus, a similar argument applies to the one made about the comparison between template sponges, in the dedicated section. Contrary to logic, the homemade sponge without any filler is the least soft by interpolating the very first linear part of the stress-strain curves (fig61e and inset). The comparison of Young's modulus evaluated in the final part of the stress-strain curves reveals that at higher compression speeds the homemade sponge is softer than the modified samples (fig61f and inset).

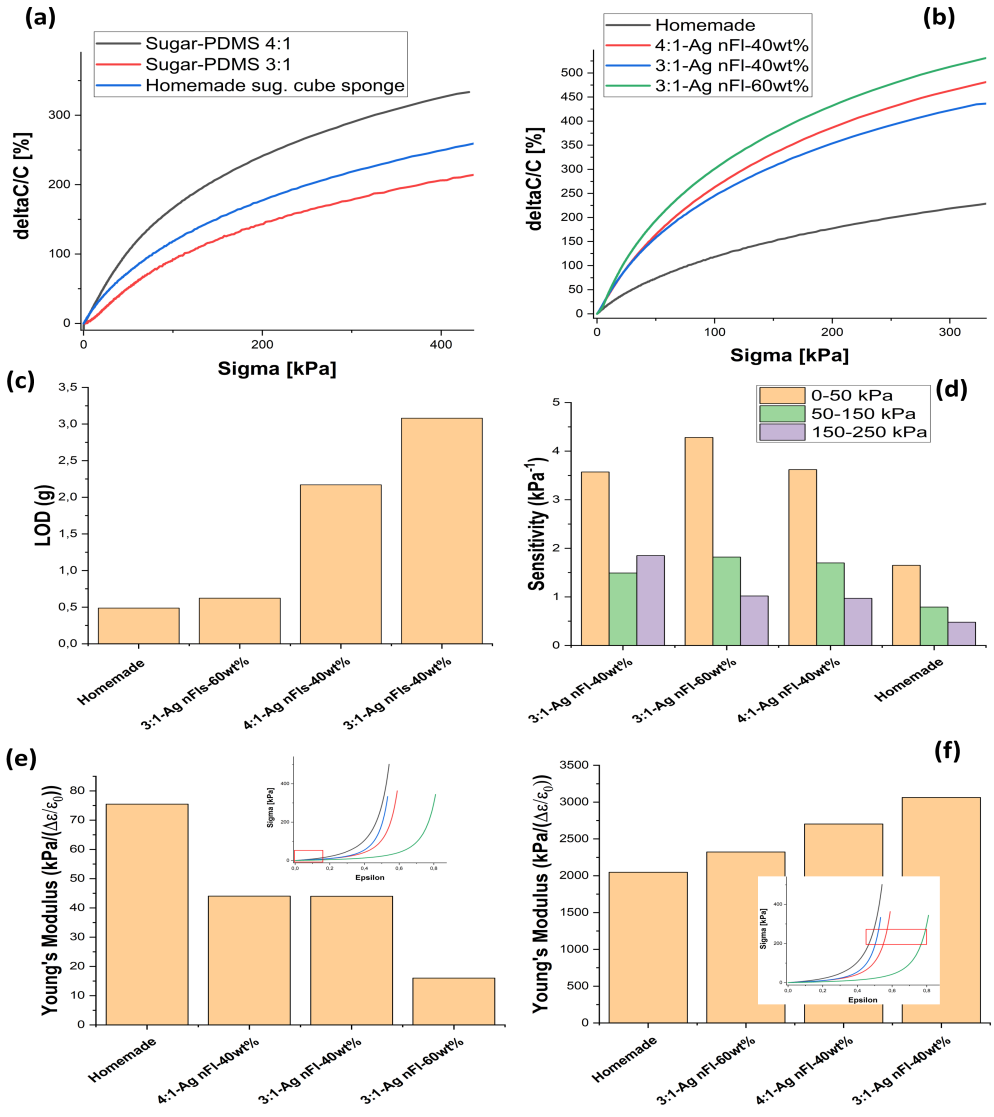

Figure 61 PDMS and sugar mix bare (Sugar-PDMS 3:1, 4:1) and modified (3:1, 4:1-Ag nFl-40wt%, 60wt%) samples compared to the homemade sugar cube one: (a, b)relative change in capacity with respect to pressure, (c)Limit Of Detection, (d)sensitivity at several pressure ranges, (e)"porous" and (f)"bulk" Young's Modulus bar graphs

8 Final comparison

Finally, the best template and mold sponges are analyzed. The combination of the PDMS and sugar mix method with the Ag nFls functionalization, not only does it give the sponge, and therefore the pressure sensor, any shape, but it greatly improves the electrical properties (fig62a) ensuring the best sensitivity in the 0-50 kPa (fig62b), while maintaining a competitive LOD (fig62c).

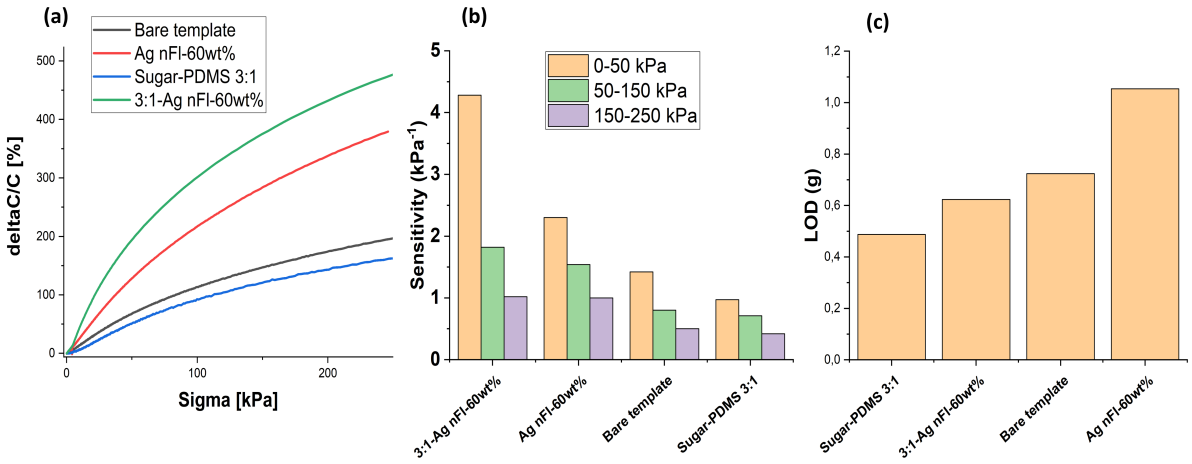

Figure 62 Comparison among the template sponges with and without Ag nFl-60% (respectively bare template and Ag nFl-60wt%), and the 3:1 sponges with and without Ag nFl-60wt% (respectively sugar-PDMS 3:1 and 3:1-Ag nFl-60wt%): (a)relative change in capacity versus pressure, (b)sensitivity and (c)LOD bar graphs

To resume, the best sample was found to be constituted by the sponge prepared with the sugar and PDMS mix method, modified with the addition of silver nanoflakes in a percentage equal to 60% of the weight of the uncured PDMS.

9 Applications

3:1-Ag nFl-60wt% sensor was finally employed as wearable device to detect physiological signals. The piezocapacitive effect was exploited to convert the mechanical deformations of the human body into electrical signals. Capacitance changes were detected by the BK precision 894 LCR meter (300 kHz of electrical frequency and 0.5 V of bias DC voltage).
A rectangular shaped sponge, almost 2 cm x 2.5 cm and 4 mm tick, obtained from the edge of a dog bone shaped sample, was the flexible core of the sensor. In order to allow the sensor to better adhere to the human body, the package described in the dedicated section was deprived of the bottom and top slides. The copper-kapton electrodes were wrapped around the sponge with a parafilm to mantain a strong physical contact.

Figure 63 3:1-Ag nFl-60% sponge with a dog bone shape. The boxed portion was the sponge employed in the wearable applications

FOTO sensore PER APPLICAZIONI WEARABLE

The removal of the slides made the electrodes conform to the sponge even during twisting and squeezing movements. Then, in order to assess the potential applicability to monitoring human signals, the sensor was wrapped around a finger for sensing bending stimuli, as shown in figure64.

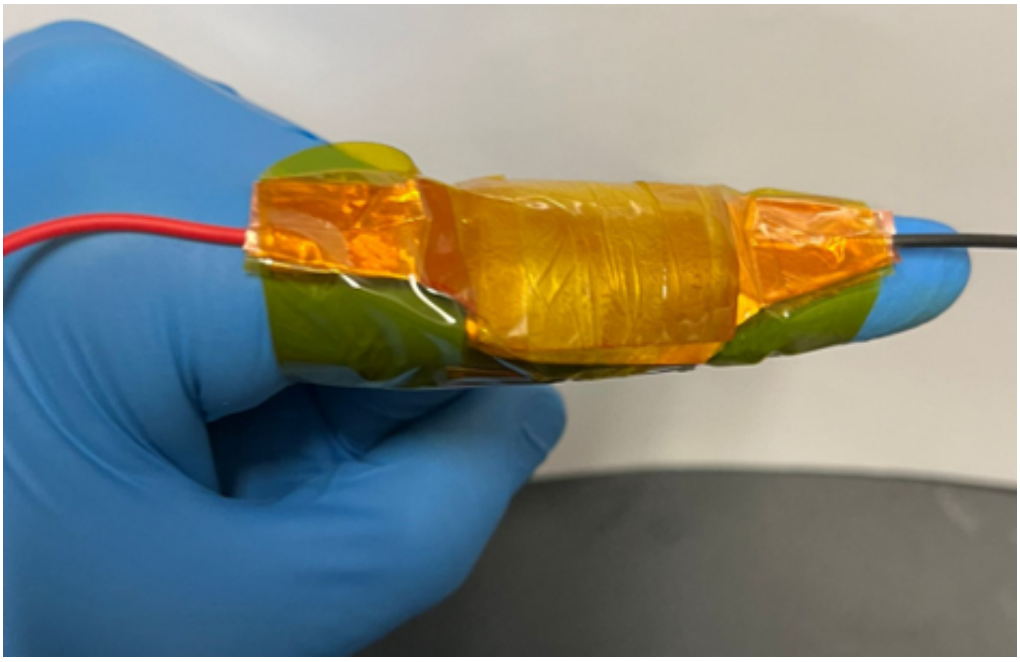

Figure 64 Packaged sponge wrapped around a finger to monitor bending

The capacitance change of the sensor is able to follow the finger progressive bending, without storing strain when it come back flat passing through the same bending angles (fig65).

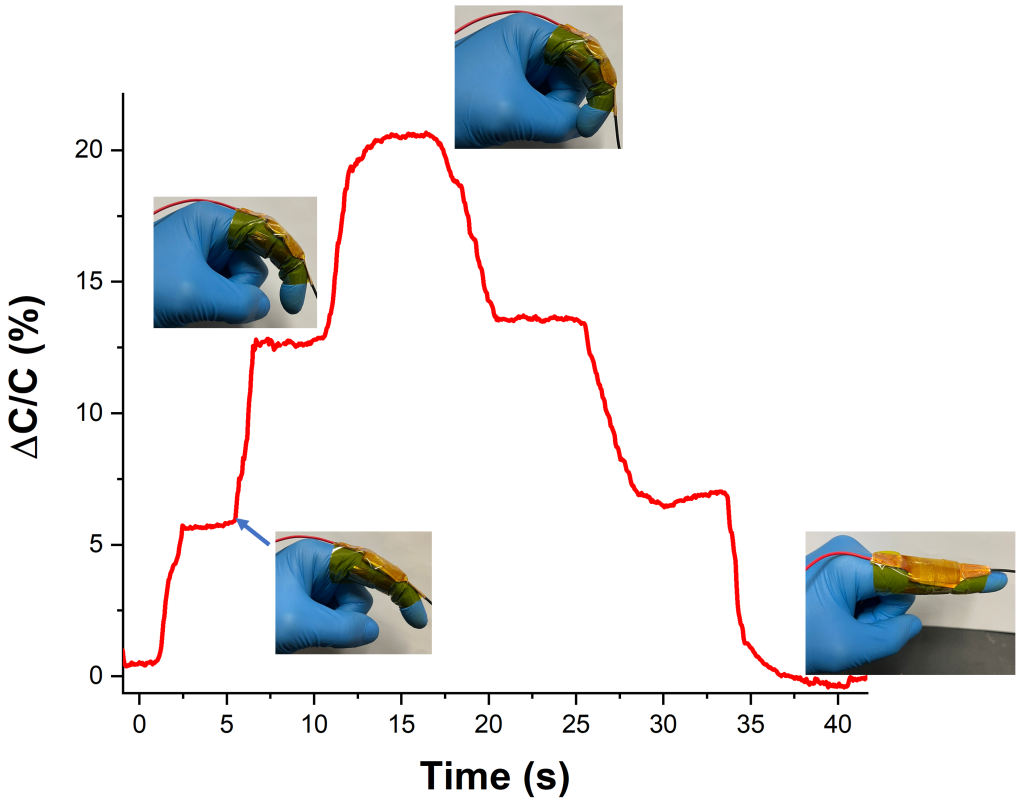

Figure 65 Relative change in capacitance over time during progressive finger bending

Successively, the bending angles have been refined and the finger was held bent for a few seconds (fig66a). A small relaxation of the $\Delta C/C$ become visible at higher angles, as pointed out by the adjacent zoom (fig66b).

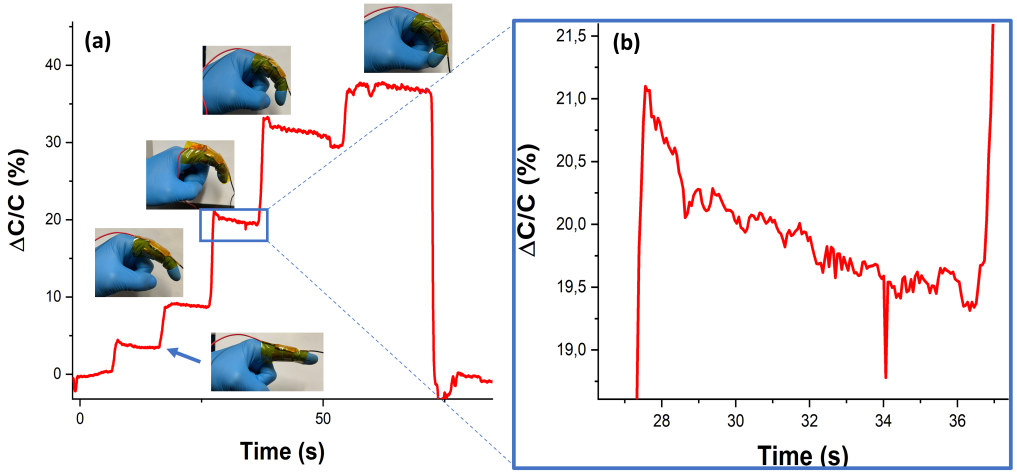

Figure 66 (a)Relative change in capacitance over time during. (b)Zoom over a relaxation mechanism

Moreover, the sensor was able to monitor the change in capacitance even as the bending speed increased, both by keeping the bending angle fixed and during its progressive enlargement (figures 67a and b, respectively).

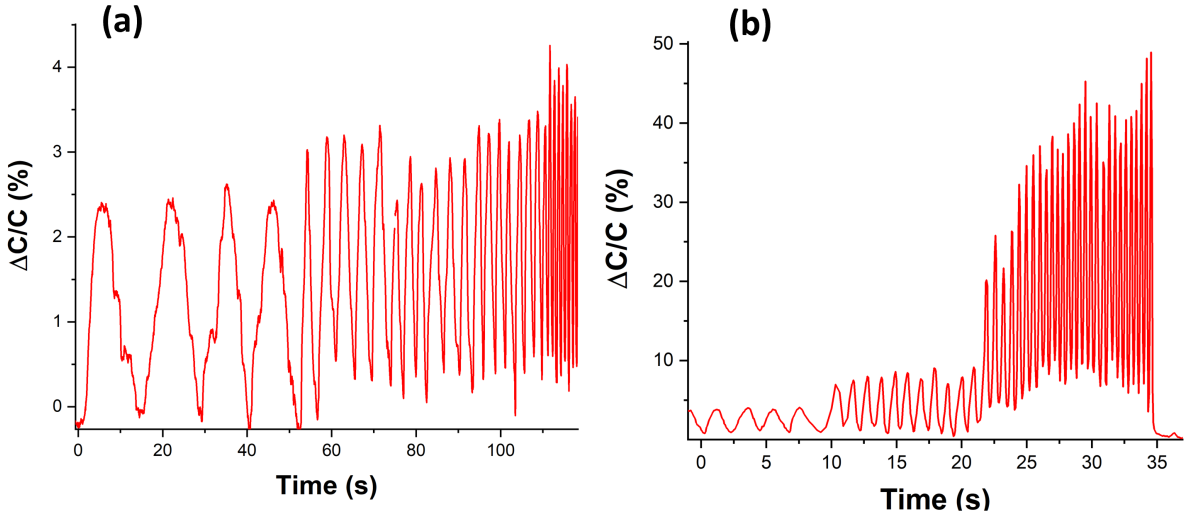

Figure 67 Relative change in capacitance over time: (a)fixed finger bending angle and increasing bending speed, (b)increasing bending angle and speed

The sensor, stuck on the throat of a volunteer (inset of figure 68a) can also measure the vibration of vocal chords while speaking. In figure 68a the pronuciation of the letter ”c” generated a peak in the capacitance signal, while whenever the word ”ciao” is pronounced, a more complex but repeating waveform is detected (fig68b).

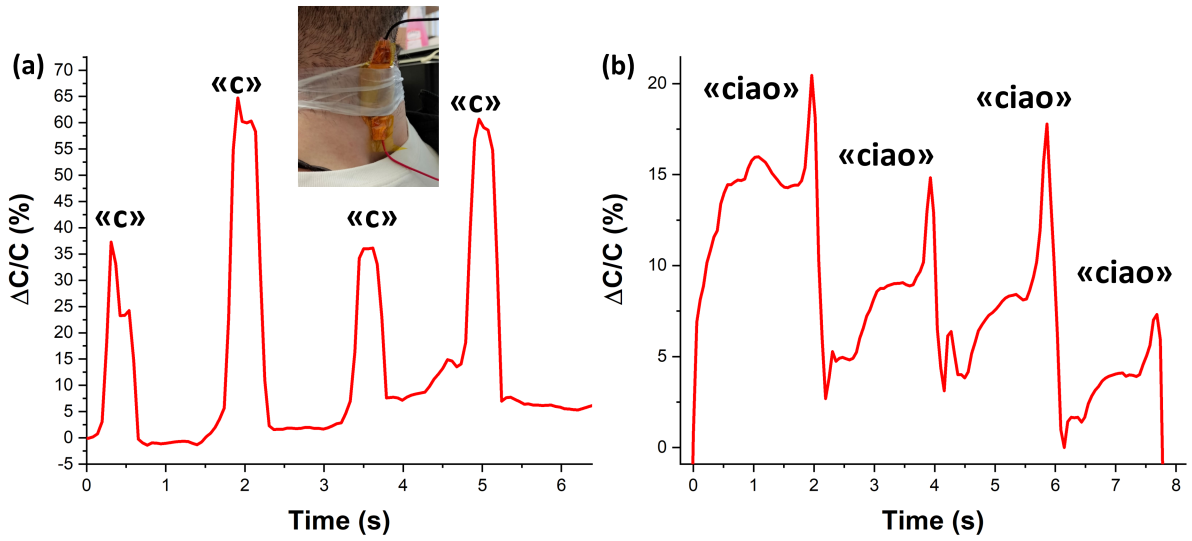

Figure 68 Relative change in capacitance over time during the pronunciation of the (a)letter ”c” and (b)word ”ciao”

10 Conclusion

In summary, here, a piezocapacitive wearable pressure sensor based on a soft and flexible polymer sponge, is investigated. The reference polymer was polydimethyloxane (PDMS) and was rendered in porous form by means of two different types of synthesis. In one case, a commercial sugar cube was used as a template. It was immersed in liquid PDMS to infiltrate it by capillarity. After a curing step to solidify the PDMS, water was used to dissolve the sugar template, resulting in a porous PDMS (pPDMS) foam with pore sizes comparable to those of the cube sugar grains, and with the same shape as the initial lump. With the aim of disregard the shape of the sponge from that of the cubic sugar template, this was replaced by common sugar powder. The liquid PDMS and the sugar powder were directly mixed together. The mixture was poured on a mold, compacted, cured and demolded. The sugar was washed away by immersion in water, resulting in a pPDMS foam, conforms to the mold used. A capacitive pressure sensor is more sensitive the greater the relative change in capacitance at a given applied pressure. The capacitance is directly proportional to the relative dielectric constant, so during the synthesis phase of the sponges, conductive nanofillers were incorporated into the polymer matrix to increase its dielectric constant and improve the performance of the devices. Two incorporation methods were explored: immersion of a ready-made sponge in a liquid solution containing a metal precursor and a priori addition of a conductive powder or a metal precursor solution together with the liquid PDMS before the curing phase. The metal precursor was silver nitrate ($AgNO_3$) while 3 different powders were tested, containing silver nanoflakes (Ag nFls), silver nanoparticles (Ag NPs) and mesoporous carbon particles (C mesoPs) respectively. Several percentage concentrations with respect to the weight of the PDMS were compared. Some sponges were also observed at the Scanning Electron Microscope to inspect the porous polymer matrix at micro and nanometer scale and check the incorporation of the conductive fillers. The samples were all packaged in the same way. The package consisted of 2 slides as top and bottom rigid planar supports for the sponge, and a couple ofcopper-Kapton foils as electrodes, each attached to an electrical wire to connect to the outside. A few wraps of parafilm kept everything in close physical contact. The packaged sensors were subjected to mechanical tests in static and dynamic mode, while an LCR meter was implemented to measure the electrical capacitance and evaluate its variation induced by mechanical pressure. The static tests involved the use of a series of weights between 1 and 50 g to be placed on the sensor in order to quantify its Limit Of Detection (LOD). The dynamic tests were performed through an Instron tensile machine used in compression mode up to an applied force of 50 N. Single run stimuli at a compression speed of $10 mm/min$ were useful to plot the relative change in capacitance ($\Delta C/C$) versus the applied pressure (or stress, σ), while cyclic compressions at $20 mm/min$ allowed to test the stability of the sensor's response and its hysteresis. All the devices demonstrated excellent stability of the electric signal, together with a negligible hysteresis in the stress-strain (σ-ε curve), during 10 compression cycles. By observing the relative variation of capacity with respect to stress, it was verified that the addition of conductive fillers actually improves the sensitivity of the devices, both in template and mold sponges. For both, silver nanoflakes were found to be the most effective fillers. The best device was the mold sponge with a 3:1 ratio of sugar to PDMS, embedded with Ag nFls at 60wt%. It shows a relative change in capacitance equal to about 600% at full scale, LOD around 6 g and sensitivity greater than $4\,\mathrm{kPa}^{-1}$ in the 0-50 kPa pressure range. This device was finally employed in a wearable application to detect physiological signals. The piezocapacitive effect was exploited to convert the mechanical deformations of the human body into electrical signals. The sensor was firstly wrapped around a finger to sense bending stimuli. It

was able to respond with a proportional electric signal to an increasing bending angle. Moreover, it successfully monitored the change in capacitance even as the bending speed increased. The sensor, stuck on the throat could also detect the vibration of vocal chords during the pronunciation of single letters or entire words.These results suggest the validity of the porous piezocapacitive sensor as a wearable strain sensor.

References

[1] URL: https://www.st.com/content/ccc/resource/sales_and_marketing/presentation/technology_presentation/group0/49/7e/8d/6c/b3/69/4a/a0/Dive_MEMS_Pressure_Sensors_Wearable_IoT_Applications/files/Dive_MEMS_Pressure_Sensors_Wearable_IoT_Applications.pdf/jcr:content/translations/en.Dive_MEMS_Pressure_Sensors_Wearable_IoT_Applications.pdf.

[2] Neil R Cameron. "High internal phase emulsion templating as a route to well-defined porous polymers". In: *Polymer* 46.5 (2005), pp. 1439–1449.

[3] Li Dan et al. "Porous polydimethylsiloxane–silver nanowire devices for wearable pressure sensors". In: *ACS Applied Nano Materials* 2.8 (2019), pp. 4869–4878.

[4] James Davies et al. "A stretchable filament sensor with tunable sensitivity for wearable robotics and healthcare applications". In: *Advanced Materials Technologies* 8.6 (2023), p. 2201453.

[5] Xuchu Dong et al. "A linear and large-range pressure sensor based on a graphene/silver nanowires nanobiocomposites network and a hierarchical structural sponge". In: *Composites Science and Technology* 155 (2018), pp. 108–116.

[6] Yuji Gao et al. "Wearable microfluidic diaphragm pressure sensor for health and tactile touch monitoring". In: *Advanced Materials* 29.39 (2017), p. 1701985.

[7] Juwon Hwang et al. "Fabrication of hierarchically porous structured PDMS composites and their application as a flexible capacitive pressure sensor". In: *Composites Part B: Engineering* 211 (2021), p. 108607.

[8] Rossella Iglio et al. "Flexible polydimethylsiloxane foams decorated with multiwalled carbon nanotubes enable unprecedented detection of ultralow strain and pressure coupled with a large working range". In: *ACS Applied Materials & Interfaces* 10.16 (2018), pp. 13877–13885.

[9] Young Jung et al. "Linearly sensitive and flexible pressure sensor based on porous carbon nanotube/polydimethylsiloxane composite structure". In: *Polymers* 12.7 (2020), p. 1499.

[10] Elgar Kanhere et al. "Flexible hydrogel capacitive pressure sensor for underwater applications". In: *Proceedings*. Vol. 1. 4. MDPI. 2017, p. 360.

[11] Elgar Kanhere et al. "Flexible hydrogel capacitive pressure sensor for underwater applications". In: *Proceedings*. Vol. 1. 4. MDPI. 2017, p. 360.

[12] Farnaz Khoshmanesh et al. "Wearable sensors: At the frontier of personalised health monitoring, smart prosthetics and assistive technologies". In: *Biosensors and Bioelectronics* 176 (2021), p. 112946.

[13] Kang-Hyun Kim et al. "Wearable resistive pressure sensor based on highly flexible carbon composite conductors with irregular surface morphology". In: *ACS Applied Materials & Interfaces* 9.20 (2017), pp. 17499–17507.

[14] Mayank Kohli et al. "Wearable Wireless Magnetic-Reluctance-Based Pressure Sensing Module for Intraoral Pressure Monitoring". In: *IEEE Transactions on Magnetics* (2023).

[15] Jin-hong Li, Jin-hui Chen, and Fei Xu. "Sensitive and wearable optical microfiber sensor for human health monitoring". In: *Advanced Materials Technologies* 3.12 (2018), p. 1800296.

[16] Siming Li et al. "Capacitive pressure sensor inlaid a porous dielectric layer of superelastic polydimethylsiloxane in conductive fabrics for detection of human motions". In: *Sensors and Actuators A: Physical* 312 (2020), p. 112106.

[17] Yunzhi Ling et al. "Disruptive, soft, wearable sensors". In: *Advanced Materials* 32.18 (2020), p. 1904664.

[18] Zhuo Liu et al. "Wearable and implantable triboelectric nanogenerators". In: *Advanced Functional Materials* 29.20 (2019), p. 1808820.

[19] Subhas Chandra Mukhopadhyay, Nagender Kumar Suryadevara, and Anindya Nag. *Wearable sensors and systems in the IoT*. 2021.

[20] Jinwon Oh et al. "Highly uniform and low hysteresis piezoresistive pressure sensors based on chemical grafting of polypyrrole on elastomer template with uniform pore size". In: *Small* 15.33 (2019), p. 1901744.

[21] Sun-Jun Park et al. “Flexible piezoresistive pressure sensor using wrinkled carbon nanotube thin films for human physiological signals”. In: *Advanced Materials Technologies* 3.1 (2018), p. 1700158.

[22] Michael S Silverstein. “Emulsion-templated porous polymers: A retrospective perspective”. In: *Polymer* 55.1 (2014), pp. 304–320.

[23] Xueqiang Tan and Jimin Zheng. “A Novel Porous PDMS-AgNWs-PDMS (PAP)-Sponge-Based Capacitive Pressure Sensor”. In: *Polymers* 14.8 (2022), p. 1495.

[24] Chi Cuong Vu, Sang Jin Kim, and Jooyong Kim. “Flexible wearable sensors-an update in view of touch-sensing”. In: *Science and Technology of Advanced Materials* 22.1 (2021), pp. 26–36.

[25] Lei Yang et al. “Structuring the reduced graphene oxide/polyHIPE foam for piezoresistive sensing via emulsion-templated polymerization”. In: *Composites Part A: Applied Science and Manufacturing* 134 (2020), p. 105898.

[26] Ruiyang Yin et al. “Wearable sensors-enabled human–machine interaction systems: from design to application”. In: *Advanced Functional Materials* 31.11 (2021), p. 2008936.

[27] Xiuhua Zhao, Fanwei Meng, and Yitian Peng. “Flexible and highly pressure-sensitive ternary composites-wrapped polydimethylsiloxane sponge based on synergy of multi-dimensional components”. In: *Composites Part B: Engineering* 229 (2022), p. 109466.